Louis S. St. Laurent **Propeller**
Damage Analyses

Prepared for
Transportation Development Centre
Transport Canada

April 2003

Prepared by:

Andrew Kendrick, P. Eng.
L. Blair Carroll, P.Eng.
Nick Pussegoda, P. Eng.
Stephanie Verbit
Kay Meyers

Submitted by:

BMT Fleet Technology Limited
311 Legget Drive
Kanata, ON
K2K 1Z8

DISCLAIMERS

This report reflects the views of the authors and are not necessarily those of the Transportation Development Centre of Transport Canada or the sponsoring organization.

The Transportation Development Centre does not endorse products or manufacturers. Trade or manufacturers' names appear in this report only because they are essential to its objectives.

Since some of the accepted measures in the industry are imperial, metric measures are not always used in this report.

PROJECT TEAM

BMT Fleet Technology Limited
Andrew Kendrick   Project Manager
L. Blair Carroll   Materials and Structures Engineer
Nick Pussegoda   Fracture and Failure Analysis Specialist
Stephanie Verbit   Mechanical Engineering Specialist
Kay Meyers   Naval Architect Student

Un sommaire français se trouve avant la table des matières.

1. Transport Canada Publication No. TP 14090E	2. Project No. 5199	3. Recipient's Catalogue No.

4. Title and Subtitle *Louis S. St. Laurent* Propeller Damage Analyses	5. Publication Date April 2003
	6. Performing Organization Document No.

7. Author(s) Andrew Kendrick, L. Blair Carroll, Nick Pussegoda, et al.	8. Transport Canada File No. 2450-C-360-4

9. Performing Organization Name and Address BMT Fleet Technology Limited 311 Legget Drive Kanata, Ontario Canada K2K 1Z8	10. PWGSC File No. MTB-1-02276
	11. PWGSC or Transport Canada Contract No. T8200-011541/001/MTB

12. Sponsoring Agency Name and Address Transportation Development Centre (TDC) 800 René Lévesque Blvd. West Suite 600 Montreal, Quebec H3B 1X9	13. Type of Publication and Period Covered Final
	14. Project Officer E. Radloff

15. Supplementary Notes (Funding programs, titles of related publications, etc.) Co-sponsored by the Program of Energy Research and Development (PERD) of Natural Resources Canada (NRCan)

16. Abstract

Two damaged propellers from the CCGS *Louis S. St. Laurent* had their deformed shapes and material properties characterized. The information was used to create non-linear finite element models of the propellers, and the models were used to derive estimates of the loads and loading mechanisms that caused the damage. Every blade was damaged while the ship was moving astern with the propellers stopped or rotating slowly. The loads derived from the analyses are considerably higher than the design loads for a ship of the *Louis S. St. Laurent's* nominal ice class, according to the load model included in the draft International Association of Classification Societies Unified Requirements for Polar Class ships.

17. Key Words Propeller damage analysis, finite element model, marine safety, design ice load, polar class icebreaker	18. Distribution Statement Limited number of copies available from the Transportation Development Centre

19. Security Classification (of this publication) Unclassified	20. Security Classification (of this page) Unclassified	21. Declassification (date) —	22. No. of Pages xviii, 46	23. Price Shipping/ Handling

CDT/TDC 79-005
Rev. 96

iii

Canada

Transports Canada **Transport Canada**		**FORMULE DE DONNÉES POUR PUBLICATION**	

1. N° de la publication de Transports Canada TP 14090E	2. N° de l'étude 5199	3. N° de catalogue du destinataire
4. Titre et sous-titre *Louis S. St. Laurent* Propeller Damage Analyses	5. Date de la publication Avril 2003	
	6. N° de document de l'organisme exécutant	
7. Auteur(s) Andrew Kendrick, L. Blair Carroll, Nick Pussegoda, et al.	8. N° de dossier - Transports Canada 2450-C-360-4	
9. Nom et adresse de l'organisme exécutant BMT Fleet Technology Limited 311 Legget Drive Kanata, Ontario Canada K2K 1Z8	10. N° de dossier - TPSGC MTB-1-02276	
	11. N° de contrat - TPSGC ou Transports Canada T8200-011541/001/MTB	
12. Nom et adresse de l'organisme parrain Centre de développement des transports (CDT) 800, boul. René-Lévesque Ouest Bureau 600 Montréal (Québec) H3B 1X9	13. Genre de publication et période visée Final	
	14. Agent de projet E. Radloff	

15. Remarques additionnelles (programmes de financement, titres de publications connexes, etc.)

Projet coparrainé par le Programme de recherche et développement énergétiques (PRDE) de Ressources naturelles Canada (RNCan)

16. Résumé

La recherche visait à caractériser les déformations de deux hélices du NGCC *Louis S. St. Laurent* ayant subi des dommages, et les propriétés de leur matériau constitutif. Les données recueillies dans le cadre de l'étude ont servi à élaborer des modèles à éléments finis non linéaires des hélices, utilisés pour calculer les contraintes estimatives et les mécanismes de surcharge responsables des dommages. Les pales des deux hélices ont été endommagées pendant que le navire était en marche arrière, hélices arrêtées ou en rotation lente. Les charges déterminées par les analyses sont beaucoup plus élevées que les charges de calcul dans le cas d'un navire de cote glace comme le *Louis S. St. Laurent*, selon le modèle de charge inclus dans le projet de norme de l'Association internationale des sociétés de classification, visant les navires de classe polaire.

17. Mots clés Analyse de dommages d'hélice, modèle à éléments finis, sécurité maritime, charge de glace de calcul, brise-glace de classe polaire	18. Diffusion Le Centre de développement des transports dispose d'un nombre limité d'exemplaires.

19. Classification de sécurité (de cette publication) Non classifiée	20. Classification de sécurité (de cette page) Non classifiée	21. Déclassification (date) —	22. Nombre de pages xviii, 46	23. Prix Port et manutention

ACKNOWLEDGEMENTS

EXECUTIVE SUMMARY

Propeller damage is an important issue for ice-capable ships. Considerable effort has been devoted to developing propeller ice load models, but there is little full-scale data available to validate these.

BMT Fleet Technology Limited (BMT FTL) obtained data on two damaged propeller blades from the CCGS *Louis S. St. Laurent*. Under contract to the Transportation Development Centre (TDC) of Transport Canada, BMT FTL used this data to create accurate models of the propeller blades and then to derive estimates of the damage loads. The loads were compared with those predicted by the latest design models as incorporated in the International Association of Classification Societies (IACS) draft Unified Requirements for Polar Class Ships. This report describes how the work was undertaken, and presents the results of the analyses and comparisons.

Samples of propeller material were taken at several places, and the inner fracture surface of one broken blade was examined in its entirety. The fracture showed no evidence of prior fatigue damage, but it was possible to identify that the fracture initiation sites were at small casting defects on the face (high pressure side) of the blade. One major fracture covered most of the failure surface, with a secondary fracture leading to the final detachment of the upper part of the blade.

The material properties of the blade near the root and close to the failure surface were characterized by chemical analysis, visual and microscopic examination, and physical testing. The properties were compared to the nominal values for the Superston 70 propeller material as quoted by the manufacturer, based on test bars. As shown in Table 1, in most cases the yield (0.2% proof) and ultimate strengths of the samples were below nominal values, often by considerable amounts.

Table 1: Tensile Properties

Specification or Specimen and Location	0.2% Yield Stress, MPa	Tensile Strength, MPa	Elongation in 50 mm Gauge Length (%)
Superston 70	310 min.*	690 min.*	18 min.*
Frac-1 (near Surface, adjacent to fracture)	338	583	20.5
Frac-2 (near Surface, adjacent to fracture)	330	578	20.5
SS-1A (near Surface, root region)	250	495	N.A[+]
SS-1B (near Surface, root region)	244	454	9.4
T/2-1A (root region)	265	519	17.5
T/2-1B (root region)	280	498	14.0
T/2-2A (root region)	221	534	19.5
T/2-2B (root region)	234	544	19.5

[+] Fracture outside the marked gauge length
* Separately cast bar

The samples from near the fracture surface were assumed to have undergone strain hardening due to the damage, and so a stress-strain cure from the root region was used in developing the non-linear finite element (FE) models. The models were created from the propeller design drawings in ANSYS 7.0, using SOLID 186 brick elements.

The damaged shapes of four of the propeller blades were captured by taking rigid polymer castings on the dockside. The castings were then measured in BMT FTL's laboratories and the measurements were used to recreate the deformed propellers. Loads were then applied to the FE models to generate matching deformations. The procedure used was iterative, and had to take account of the fact that the castings represent the residual deformations of the blades rather than the peak deformations under the applied loads. In all cases, it was possible to achieve a reasonably good match between the castings and the FE models, as shown in Figure 1. The casting and FEA models coincide over the bulk of the blade surface.
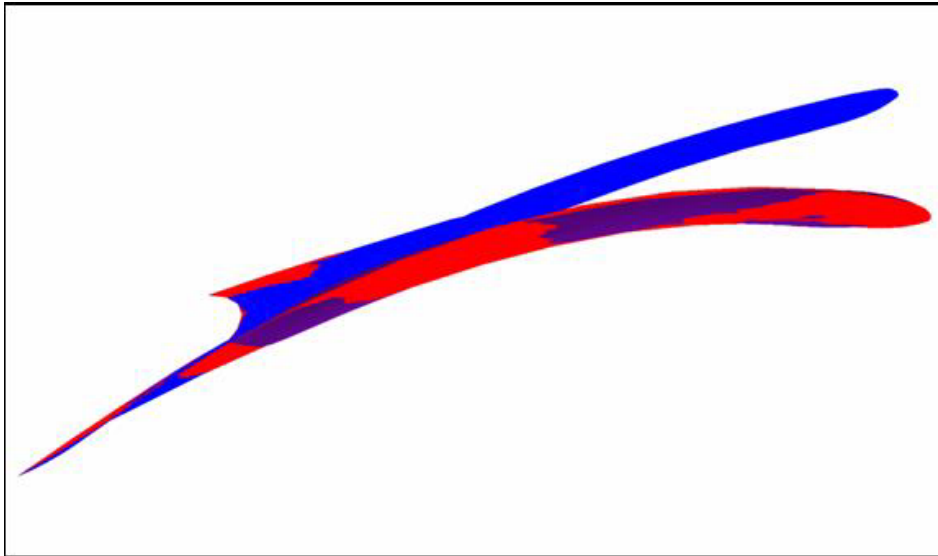

Figure 1: Original Starboard Blade + Blade 1 Casting + FEA Rebounded Model

The loads required to produce the deformations are summarized in Table 2. The total loads are considered to be reasonably accurate, while the areas and pressures may be less so. However, the pressure/area data is quite consistent with other ice load data. For all four blades that were successfully analyzed, the stresses under the applied load exceeded the material yield strength over much of the blade, and approached ultimate for the most highly loaded blades.

Table 2: Summary of Applied Loads

Blade		Loaded Area (m²)	Average Pressure (MPa)	Total Load (MN)
Starboard	1	0.460	8.04	3.68
	2	0.295	9.22	2.92
	3	0.356	9.22	3.28
Port	4	0.432	5.16	2.23

For comparison, the design ice load for the *Louis S. St. Laurent*, assuming her to be approximately a PC3 ship under the new IACS classes, is in the order of 2 MN. This design load would also be applied in a completely different pattern to that derived from the analyses. The design loads are based on the ship moving ahead into the ice, while the damage loads from the *Louis S. St. Laurent* are from an incident where the ship appears to have been backing into heavy ice with propellers stopped or turning slowly. The backing scenario is known to be very hazardous, and the results of the project emphasize this.

An analysis of the blades under the nominal design loads showed that their strength would be considered inadequate if the actual material properties were used in the calculations, but marginally acceptable if nominal properties were used. This has implications both for design and for analysis of performance. It is crucial that all calculations incorporate realistic values for material properties.

The innovative forensic analysis toolset used in the project was shown to be capable of deriving a good understanding of damage mechanisms and reasonably confident estimates of damage loads for bending damage. In the future, if other propellers are damaged by ice milling or other "design-type" scenarios, the toolset would be able to test the loading assumptions in design rules more directly.

SOMMAIRE

Les dommages aux hélices peuvent avoir des conséquences graves pour les navires évoluant dans des eaux envahies par les glaces. Malgré les efforts considérables consacrés à l'élaboration de modèles de charges de glaces imposées aux hélices, il existe peu de données en vraie grandeur permettant de valider ces modèles.

BMT Fleet Technology Limited (BMT FTL) a colligé des données sur deux pales endommagées provenant du NGCC *Louis S. St. Laurent*. En vertu d'un contrat passé avec le Centre de développement des transports (CDT) de Transports Canada, BMT FTL a exploité ces données pour créer des modèles précis des pales des hélices, puis calculé des valeurs estimatives des charges ayant causé des dommages. Les charges calculées ont ensuite été comparées avec celles prédites par les derniers modèles incorporés dans le projet de normes sur l'utilisation des navires dans les eaux recouvertes de glace de l'Arctique, de l'Association internationale des sociétés de classification. Le présent rapport décrit les travaux de la recherche en plus de présenter les résultats des analyses et des comparaisons.

Des éprouvettes du matériau de l'hélice ont été prélevées en plusieurs points. La surface interne de rupture d'une des pales a été complètement examinée. Même si la cassure ne démontrait aucun signe de dommage antérieur par fatigue, on a pu déterminer que les sites de déclenchement de rupture coïncidaient avec des petits défauts de coulée sur la face de la pale (côté haute pression). Une cassure majeure couvrait presque toute la surface de rupture, une seconde cassure s'étendant jusqu'à la séparation finale de la partie supérieure de la pale.

Les caractéristiques du matériau de la pale près de l'emplanture et près de la surface de rupture ont été déterminées par analyse chimique, examen visuel, examen microscopique, et par des tests physiques. Les propriétés ont été comparées aux valeurs nominales indiquées par le fabricant pour le matériau Superston 70 utilisé pour l'hélice. Comme on peut le constater dans le tableau 1, dans la plupart des cas, la limite d'élasticité (0,2 %, valeur d'épreuve) et la résistance maximale des éprouvettes étaient inférieures, parfois de beaucoup, aux valeurs nominales.

Tableau 1 : Caractéristiques de traction

Spécification/éprouvette et emplacement	Limite d'élasticité (0,2 %) MPa	Résistance à la rupture MPa	Allongement (%) distance entre repères de 50 mm
Superston 70	min. 310*	min. 690 *	min. 18*
Frac-1 (près de surface, contiguë cassure)	338	583	20,5
Frac-2 (près de surface, contiguë cassure)	330	578	20,5
SS-1A (près de surface, emplanture)	250	495	N/D[+]
SS-1B (près de surface, emplanture)	244	454	9,4
T/2-1A (emplanture)	265	519	17,5
T/2-1B (emplanture)	280	498	14,0
T/2-2A (emplanture)	221	534	19,5
T/2-2B (emplanture)	234	544	19,5

[+] Cassure dépassant la distance entre repères

* Éprouvette coulée distincte

On a présumé que les éprouvettes à proximité de la surface de rupture avaient subi un durcissement par écrouissage, et utilisé un diagramme effort-déformation de la zone d'emplanture pour élaborer les modèles à éléments finis non linéaires. Les modèles ont été créés à partir des dessins d'étude des hélices, avec logiciel ANSYS 7.0, en utilisant des éléments en pavés SOLID 186.

Pour saisir les profils endommagés de quatre pales d'hélice, des moulages en polymère rigide ont été pris à quai. Les moulages ont été ensuite mesurés dans les laboratoires de BMT FTL et les résultats ont servi à recréer les hélices déformées. Des charges ont été appliquées aux modèles à éléments finis pour générer des déformations correspondantes. Les chercheurs ont alors utilisé pour cela une méthode itérative, et ils devaient tenir compte du fait que les moulages représentaient les déformations résiduelles des pales plutôt que les pics de déformations sous les charges appliquées. Il a été possible dans tous les cas de réaliser une correspondance relativement bonne entre les moulages et les modèles à éléments finis, comme l'illustre la figure 1. Le moulage et les modèles d'analyse par éléments finis (AEF) coïncident avec la majeure partie de la surface de la pale.
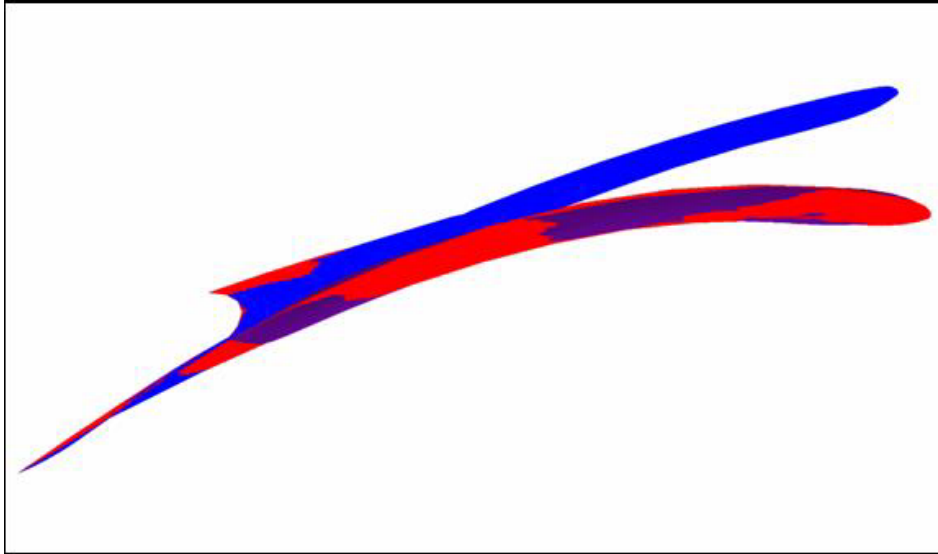
Figure 1: **Pale d'hélice tribord originale + Moulage de pale 1 + Modèle AEF
du retour élastique**

Le tableau 2 contient les charges requises pour produire les déformations. On estime que les valeurs des charges totales sont raisonnablement précises, alors que les valeurs de surfaces et de pressions peuvent l'être moins. Or, les données de pression de surface correspondent passablement aux autres données sur les charges de glace. Pour les quatre pales analysées avec succès, les contraintes sous la charge appliquée sont supérieures à la limite élastique de la majeure partie de la pale, et se rapprochent de la résistance maximale dans le cas des pales les plus chargées.

Tableau 2 : Sommaire des charges appliquées

Pale		Surface en charge (m^2)	Pression moyenne (MPa)	Charge totale (MN)
H. tribord	1	0,460	8,04	3,68
	2	0,295	9,22	2,92
	3	0,356	9,22	3,28
H. bâbord	4	0,432	5,16	2,23

Aux fins de comparaison, la charge de glace de calcul applicable au *Louis S. St. Laurent*, en supposant que celui-ci est désigné navire de classe polaire 3 selon la nouvelle classification de l'Association internationale des sociétés de classification, est de l'ordre de 2 MN. Cette charge de calcul serait également appliquée selon un mode totalement différent de celui résultant des analyses. Les charges de calcul concernent un navire évoluant dans les glaces, alors que les charges responsables des dommages aux hélices du *Louis S. St. Laurent* résultent d'un incident survenu alors que le navire, vraisemblablement, faisait marche arrière dans des glaces denses, hélices arrêtées ou tournant à faible vitesse. La marche arrière est évidemment très risquée, ce que font ressortir les résultats de la recherche.

Une analyse des pales soumises aux charges de calcul nominales a démontré que leur résistance serait considérée inadéquate si on utilisait les propriétés réelles du matériau pour les calculs, mais qu'elle serait acceptable par une faible marge en utilisant les propriétés nominales. Cette constatation a des répercussions tant pour le calcul que pour l'analyse des performances. Il est primordial que tous les calculs soient faits avec des valeurs réalistes quant aux propriétés du matériau.

La boîte d'outils innovatrice d'analyse de contrôle utilisée pour le projet a permis d'acquérir une bonne connaissance des phénomènes de dommages et d'évaluer avec un niveau de confiance raisonnable les charges de dommages causant des flexions. À l'avenir, si d'autres hélices sont endommagées lors d'opérations de broyage de glace ou dans d'autres conditions-types, les outils d'analyse pourraient permettre de vérifier plus directement les hypothèses de chargement comprises dans les règles de conception.

TABLE OF CONTENTS

LIST OF FIGURES

LIST OF TABLES

GLOSSARY

ASTM	American Society of Testing Materials
CCGS	Canadian Coast Guard Ship
FE	Finite Element
FEA	Finite Element Analysis
HP	high pressure (face)
IACS	International Association of Classification Societies
IPC	inductive couple plasma
JRPA	Joint Research Project Agreement
kN	kilonewton
LP	low pressure
LPI	liquid penetrant inspection
m	metre
Mn	magnesium
MN	meganewton
MPa	megapascal
NDE	Non-destructive Examination
NIST	National Institute of Standards and Technology
NRC	National Research Council Canada
RPM	revolutions per minute
SNAME	Society of Naval Architects and Marine Engineers
TC	Transport Canada
TDC	Transportation Development Centre
UR	Unified Requirement

1.   INTRODUCTION

Propeller strength is a key issue for ice-capable ships. Damage to propellers in ice is not uncommon. It can lead to immobilization of the ship, requiring costly and sometimes hazardous intervention. On occasion, it may put the ship itself at risk if conditions are dynamic and/or worsening.

On the other hand, if propellers are made unnecessarily strong, they are expensive to manufacture and will lose propulsive efficiency due to thicker, less efficient sections, increasing the operational cost and the environmental impact. Excessively strong propellers may lead to damage farther along the shaft line, with even more undesirable effects. It is essential to strike the correct balance. Canada has undertaken significant work in this area, notably the Joint Research Project Agreement (JRPA) 6 with Finland, which has led to the development of a design model for inclusion in national (Finnish/Swedish) and international (IACS Unified Requirements) standards. A limited amount of full-scale data has been collected to support this model.

The project described herein was intended to test a technique for establishing extreme ice loads by forensic analysis of damaged propeller blades, taken in this case from the CCGS *Louis S. St. Laurent*. Several aspects of the project were unique and highly innovative.

The project was undertaken by BMT Fleet Technology Ltd (BMT FTL) under a contract with the Transportation Development Centre (TDC) of Transport Canada (TC). TC also provided support for the collection of material samples prior to the main project. Within BMT FTL, several parts of the organization contributed to the work, which required a multi-disciplinary approach.

This report provides details of the project's background and objectives. Descriptions are provided of the work that was undertaken, including measurement of the damaged propellers, characterization of samples of propeller material, and the finite element modelling of each damaged blade. Hypotheses as to the cause(s) of the damage that was experienced are presented, and compared with the propeller design load models included in various rule and requirement systems. Recommendations are made as to how future projects could benefit from the work and from its extension to other damage analysis.

2. BACKGROUND AND OBJECTIVES

2.1 Background

Propeller damage is one of the most frequent forms of ice damage for ice-going ships [1]. Design standards for propellers are therefore an important component of construction standards. A considerable amount of research and development in this area has been undertaken, principally in Canada, Finland, and Russia over the last decade. This has resulted in new requirements for Baltic Class ships [2] and draft International Association of Classification Societies (IACS) Unified Requirements [3], both based in large part on the work of the JRPA 6 between Canada and Finland [4]. JRPA 6 produced an ice-loading model, which was then used to derive a set of design requirements.

The load model from JRPA 6 is not universally accepted, as it is based on limited and somewhat ambiguous full-scale data. Further validation work is therefore required, and some of this has been undertaken as described below. However, all dedicated ice tests and trials are difficult and expensive, and some good fortune is needed to ensure that the results obtained meet the objectives.

The concept of using forensic analysis of propeller damage to supplement available data is based on some success in using similar approaches to validate hull structure requirements. Although it is not always known precisely when damage occurred, or what the ice conditions were at the time, the fact that some type of overload took place is very important knowledge. Furthermore, it has been possible to use the damage pattern to test hypotheses regarding load magnitudes and distributions.

Applying this approach to analysis of propeller damage is more challenging, as there are more unknowns and more important parameters than in the case of hull structure – for example, the range of possible impact speeds and directions is much greater due to propeller rotation. However, it was believed that a pilot project could be of great benefit in exploring the potential of the approach and, hopefully, in providing new insights into damage load mechanisms.

2.2 Prior Experience and Work on CCGS *Louis S. St. Laurent*

The CCGS *Louis S. St. Laurent* (the "*Louis*") remains Canada's largest and most powerful icebreaker, some 35 years after her entry into service.

The original propeller design for the *Louis* used a manganese bronze material and proved to be inadequate to the needs of Arctic service. Numerous fractures and blade deformations were experienced on a series of propellers before their recent replacement with a new design fabricated in stainless steel. The overall design characteristics of the old propeller are as shown in Table 2.1.

Table 2.1: Propeller Particulars

LOUIS S. ST. LAURENT
Propeller Particulars

Diameter (m)	4.57
Number of Blades	4.00
Pitch (m)	3.42
Pitch Ratio	0.75
Expanded Area (m2)	9.12
Expanded Area Ratio	0.552
Rotational speed (bollard)	133/139
Weight (approx) (kg)	14216

In the last season of operation of the old propellers, an optical measuring system was installed on the ship and captured a certain amount of load data. However, the system was not capable of determining loads beyond first yield. For this and other reasons, it did not capture the events that led to damage to two of the propellers during the voyage, one of which suffered a blade fracture.

The optical system has now been used with the new propellers, which have not (yet) yielded. The lack of top-end data on the old propellers means that extreme loads on the two designs cannot be compared. If this were possible, then the predicted influence of parameters such as blade area ratio, pitch, RPM, etc. could be verified.

Moulds of the damaged blades of two old design propellers (Figure 2.1) were taken and material samples were collected by BMT FTL, with partial funding support from TC. The moulds and samples provide the essential data for the work in this project.

Figure 2.1: Damaged Propellers

The technique of taking moulds is one that BMT FTL has used extensively in damage analysis of pipelines, notably for dents. A compound is applied to the surface and cures to provide a rigid mould that can be 'peeled' away from the metal surface and brought to a laboratory for accurate definition of shape. Figure 2.2 shows the mould on the face (aft, or high pressure side) of one propeller blade.

The moulds created for the propellers were much larger than typical pipeline moulds, and some problems with curing were experienced due to the high temperatures and humidity on site. This also meant that more compound had to be used to provide a rigid mould than had been expected when the materials were ordered. Therefore, from eight potential blades only five useable moulds were produced, one of which was for the blade that had fractured.   This still provided a substantial amount of potential information.

Figure 2.2: Mould on Propeller Blade

2.3   Objectives

The principal objectives of the current project were:

- to determine the extreme loads seen by the propellers of the *Louis* during the 1999 Arctic deployment; and
- to compare these with the loads on the new design and the predictions of the IACS UR/JRPA 6 load model.

The secondary objectives included:

- definition of the post-yield, fatigue, and fracture performance of the bronze material; and
- characterization of the failure modes.

These objectives were to be accomplished through a series of tasks as listed below.

Task 1: Fracture examination and material property characterization
Task 2: Propeller finite element model development
Task 3: Damage analysis and load definition
Task 4: Correlations with IACS Unified Requirement Load Model
Task 5: Reporting

As will be discussed in detail, Task 4 could not be accomplished meaningfully based on the outcome of the previous tasks, as all the damages to the two propellers involved scenarios not covered by the IACS model. This in itself is an important result.

3. TASK 1: FRACTURE EXAMINATION AND MATERIAL CHARACTERIZATION

3.1 Introduction

The objective of this task was to determine bulk material composition and mechanical properties for material classification and also as an input for the material model for Finite Element Analysis (FEA), respectively. Two samples taken from the propellers were available. One was taken near the root, where the material is assumed to have remained elastic. The other encompasses a fracture surface from a failed blade, and may have yielded before fracture.

In addition, the fracture surface was examined visually to locate fracture initiation site(s) to see whether there was evidence of fatigue crack growth, internal (casting) defects, or other features that may have contributed to failure. This information would be useful in defining ultimate failure criteria.

3.2 Findings

3.2.1 Fracture Surface Examination

The fracture surface examination indicated two initiation points. One of these points was associated with a casting defect (see Figure 3.1(a)), while the other initiation point appeared to be close to another casting defect visible at macroscopic level. At this level of magnification, the chevrons associated with this portion of the fracture point to a location that is not coincident with this visible defect (Figure 3.1(b)).

The majority of the fracture propagation took place from the initiation point shown in Figure 3.1(a). Figure 3.2 is an inverted view of the fracture with respect to the view in Figure 3.1, at a lower magnification. It clearly displays the major propagation event as evident from the apex of the chevrons that point towards the initiation site. It is apparent from Figure 3.2 that the fracture initiation point is on the face (high pressure (HP) side) of the blade. The same is true for the second initiation point shown in Figure 3.1(b).

Macroscopic scales are normally best for observing fatigue crack growth. In this case there is no evidence of fatigue crack growth associated with the brittle fracture initiation. As there is no visible link to a defect (flaw) for the second initiation site, this region was subject to closer and higher magnification forensics. The local fracture initiation region marked by the black arrow in Figure 3.1(b) was cut out for this purpose. The fracture surface was cleaned in 50/50 HCl/distilled water solution with Rodine as an inhibitor to remove any oxide. Examination performed with the aid of the stereoscope indicated the initiation was indeed linked with a smaller casting defect. Figure 3.3 shows the cut out sample with the arrow pointing to the fracture initiation point (black arrow). Also observed on the extracted sample is a surface layer of metal, 2 to 4 mm thick, on the surface of the propeller blade that has a different texture than the rest of the fracture.

(a)

(b) white arrow points to a casting defect.

Figure 3.1: Fracture Initiation Points

Note: Fracture initiation points are marked by black arrows. The yellow substance on the fracture surface is a remnant of the molding material.

Figure 3.2: Lower Magnification of the Fracture

Note: The chevrons indicate the direction of fracture propagation to the right. The white arrow points to the initiation region and the black arrow in Figure 3.1(a) marks the initiation point.
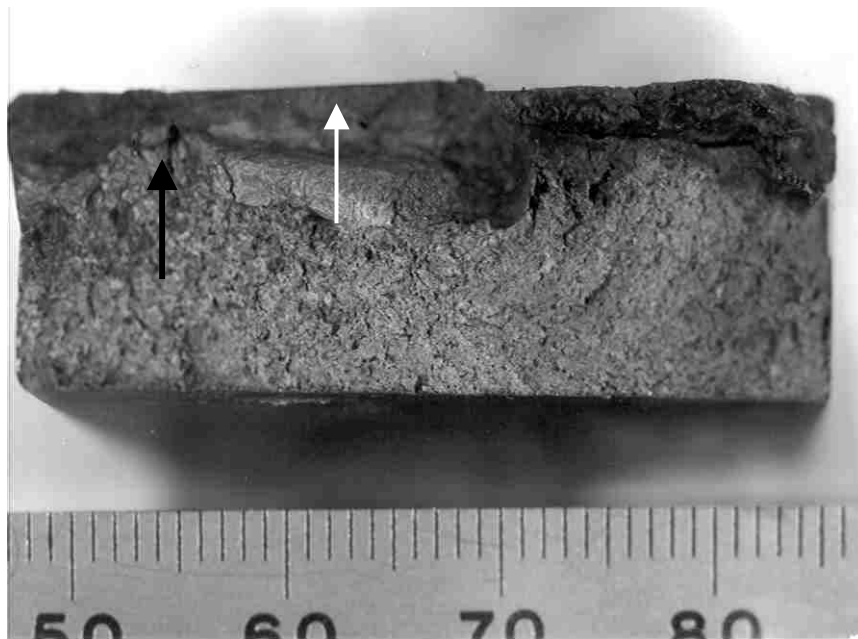

Figure 3.3: Close-up of Fracture Initiation Region in Figure 3.1(b)

Note: The HP side of the blade is on top. The layer of metal with a different texture is shown by the white arrow.

A close-up of the main initiation point in Figure 3.1(a) is presented in Figure 3.4. The black arrow identifies the associated casting defect. Once again, a different texture is observed on some regions of the surface.
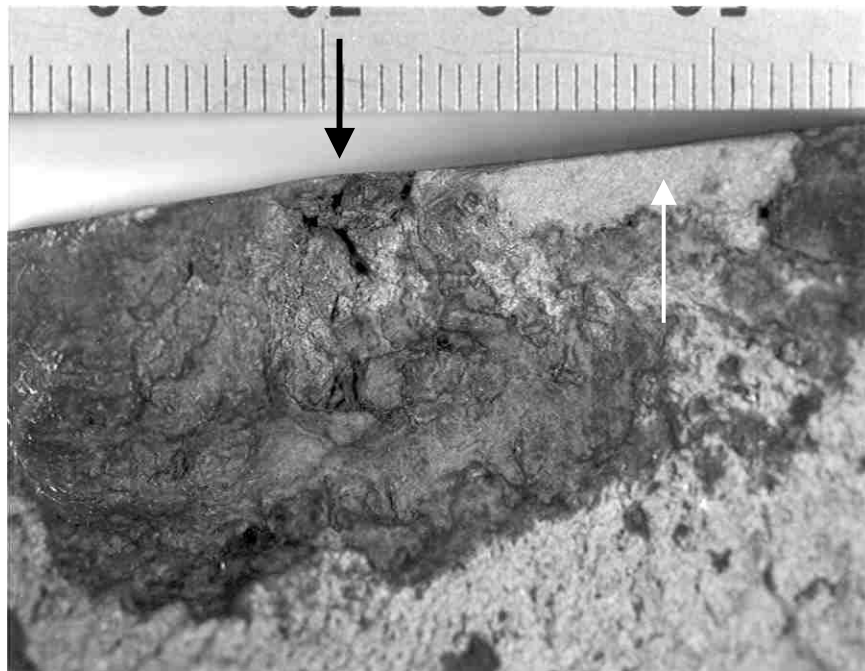

Figure 3.4: Close-up of Fracture Initiation Region in Figure 3.1(a)

Note: The layer of metal with a different texture is shown by the white arrow.

A previous examination of a propeller blade fracture on the CCGS *Louis S. St. Laurent* [5], resulting during operation in ice, showed that this incident was a result of brittle fracture that initiated from casting defects. The propeller material was a Mn-bronze (Superston 70) blade. The fracture took place at 0.63 of the pitch radius, and the initiation sites were, by contrast, on the low pressure (LP) side (the back of the blade). Several small subsidiary cracks parallel to the main fracture were observed on the LP side, and mechanical testing of specimens extracted from the sub-surface location on the LP side indicated that the region close to the fracture was plastically deformed well beyond the yield strength.

Figure 3.5 displays an example of the subsidiary cracks on the HP side (the face) of the blade in the current investigation. By contrast, there was no cracking observed on LP side of the blade close to the fracture at macroscopic levels (see Figure 3.6).

Figure 3.5: Examples of Cracks Close to the Fracture on the HP Side of the Blade

Figure 3.6: View of the HP Side of the Blade Adjacent to Fracture

3.2.2   NDE Examination of the Blade Surface Adjacent to Fracture

This task was performed to assess the degree of cracking first observed by visual inspection. This information could assist in defining ultimate failure criteria (e.g. safe crack sizes) from a fracture mechanics perspective. Therefore, the largest surface cracks detected were later broken open using liquid nitrogen. Liquid penetrant inspection (LPI) was conducted and the results are presented in Figure 3.7. The method, as expected, was able to detect tight cracks not visible to the naked eye.

Figure 3.8 shows the results of LPI on the LP side. Linear crack-like flaws were not detected on this side of the blade surface. Only some indications of surface imperfections, perhaps cavities and surface damage from handling or operation, were detected.

The layer in the fracture surface close to the blade surface is very fine and does not represent the rest of the fracture surface of the blade. This could be representative of "dressing"/weld repair of the blade surface.

3.2.3   Mechanical Testing and Material Characterization

Extraction of Samples

The blade sample taken nearest the root, where the material is assumed to have remained elastic, was chosen for extensive testing and material identification. Within the cut out in Figure 3.10, the two regions selected for the extraction of test specimens are marked. The tensile test specimens were extracted with their loading axis parallel to the marked lines. Comparison is made below with test results from the tensile properties at the fracture initiation region. An objective is to assess the degree of plastic deformation that occurred before fracture.

Two sets of tension specimens were extracted from the location marked by the solid line – one set sub-surface and the other at mid-thickness – with the objective of assessing any through thickness cooling rate effects on mechanical properties. The specimens extracted from the location indicated by the broken line at the mid-thickness location were selected to determine tensile properties at a slower cooling rate of material available in the elastic state with lesser likelihood of damage from loading. In all cases, duplicate specimens were machined and tested to ensure that any effect of cooling rate, location and strain condition was captured (outside the normal range of specimen-to-specimen variation). The tests specimens had a standard 12.5 mm diameter and 50 mm gauge length and were tested at the quasi-static loading rate in accordance with ASTM E8:1997 at room temperature.

Blanks for extracting Charpy specimens were extracted from the same locations as the tensile test specimens. A through thickness notch orientation was used to produce fracture orientations representative of the fracture propagation direction in the blade. Three standard full-size Charpy specimens (ASTM E23:1997) were machined from each location and tested in a NIST calibrated 400 J machine.

(a)
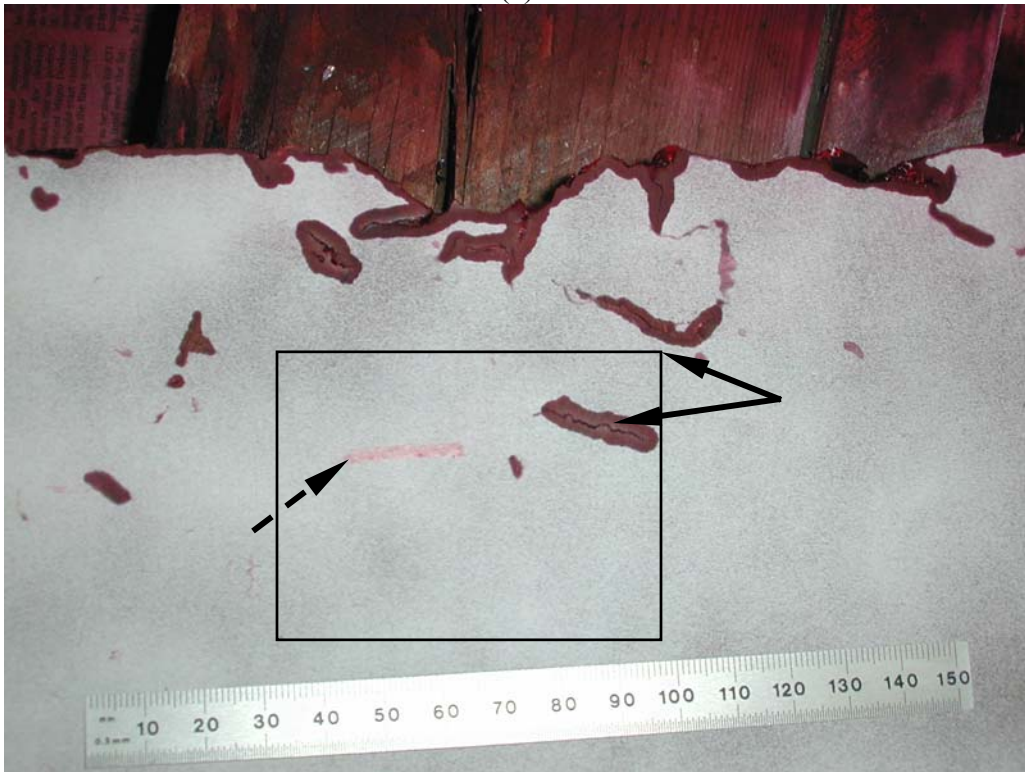
(b) same region shown in Figure 3.5, and the two arrows show the cracks visible in Figure 3.5, while the dashed arrow shows a new detection.

Figure 3.7: LPI Results on the LP Side of the Blade

Figure 3.8: LPI Results on the HP Side of the Blade

Note: Mechanical damage is marked by the arrow.

The attempt to open up the large crack after immersion in liquid nitrogen was successful as presented in Figure 3.9. The darker region is the "pre-existing crack" and the bright region is the brittle fracture surface produced when breaking the specimen. A different texture of the fracture surface is seen adjacent to the blade surface similar to those presented in Figures 3.3 and 3.4.
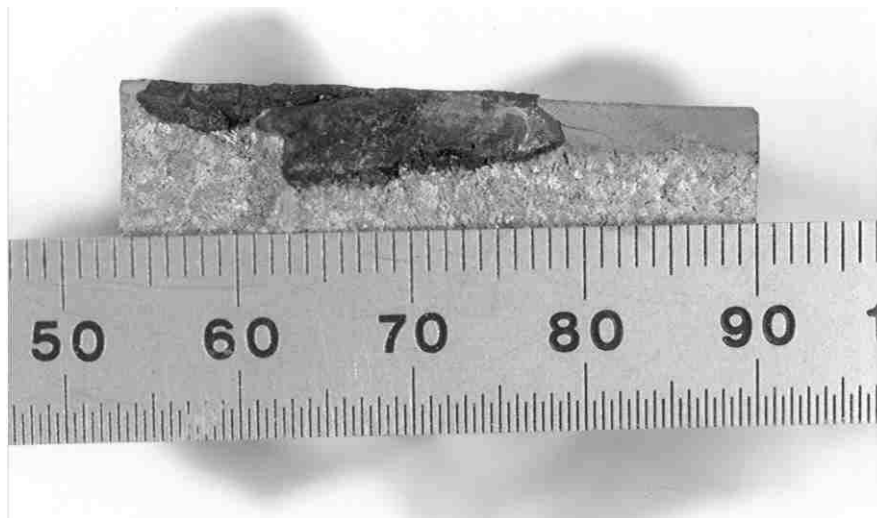

Figure 3.9: Fracture Sample Produced at Liquid Nitrogen Temperature

Note: A layer of metal with a different texture can be seen at the blade surface.
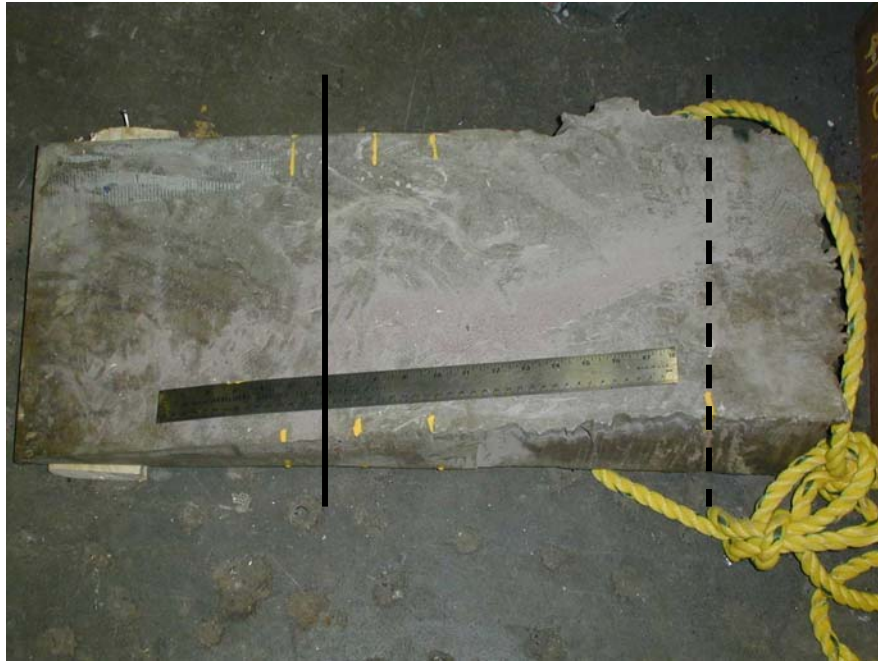
Figure 3.10: Specimen Extraction from Root Region of the Blade

Samples for chemical analysis were taken from material extracted from two locations for the root region of the blade. One specimen from the sub-surface location (marked by the solid line) and the other from the mid-thickness of the location (marked by the broken line) identified in Figure 3.10 were analyzed at Bodycote Materials Testing Canada Inc., Burlington, Ontario. The method employed used inductive couple (argon) plasma (IPC) instrumentation. The results are presented in Table 3.1.

Tensile and Charpy specimens were extracted from the fracture initiation region just below the surface where the residual strain was expected to be the highest from bending loads. The procedure employed was the same as described for specimens machined from the root region. The test samples were taken from the area of maximum thickness of the blade at this radius. In the previous work this approach was considered to have been successful in determining the strain damage before fracture occurred [5].

Test Results: Chemical Analysis

Table 3.1: Chemical Composition of the Blade Material (wt%)

Element	Superston 70	Near Surface	Mid-Thickness
Cu	71 min	73.91	72.41
Fe	2.0 to 4.0	2.62	4.21
Mn	13.5 – 15.5	13.67	13.71
Ni	1.5 - 2.5	1.84	1.89
Pb	0.05 max.	0.010	0.011
Al	7.0 - 8.2	7.86	7.77

The results from chemical analyses generally conform to those specified by Stone Marine for Superston 70 alloy. The only non-conformance is the Fe content of 4.21 from the mid-thickness location, and this could be result of segregation in the centre of the blade that is usually the last region to solidify.

Test Results: Tensile Test Results

Table 3.2: Tensile Properties

| Specification or Specimen and Location	0.2% Yield Stress, MPa	Tensile Strength, MPa	Elongation in 50 mm Gauge Length(%)
Superston 70	310 min.*	690 min.*	18 min.*
Frac-1 (near Surface, adjacent to fracture)	338	583	20.5
Frac-2 (near Surface, adjacent to fracture)	330	578	20.5
SS-1A (near Surface, root region)	250	495	N.A[+]
SS-1B (near Surface, root region)	244	454	9.4
T/2-1A (root region)	265	519	17.5
T/2-1B (root region)	280	498	14.0
T/2-2A (root region, broken line Fig. 9)	221	534	19.5
T/2-2B (root region, broken line Fig. 9)	234	544	19.5

[+] Fracture outside the marked gauge length
* Separately cast bar

None of the tensile test results from the blade meet the minimum strength requirements for separately cast bars. This is primarily a result of the higher cooling rate of separately cast bars. The duplicate specimens from the fracture region display a higher strength compared to the results from specimens extracted from the root region of the blade. Here, the best comparison would be with subsurface specimens from the root region, where the damage from loading is expected to be minimal. If the yield strengths are compared, the average increase in strength is about 35%. Figure 3.11 shows the initial part of the engineering stress-strain curves for two of the specimens – one specimen extracted nearest the root and one from the fracture region. The elevated flow curve for the specimen from the fracture region is possibly a result of work hardening.
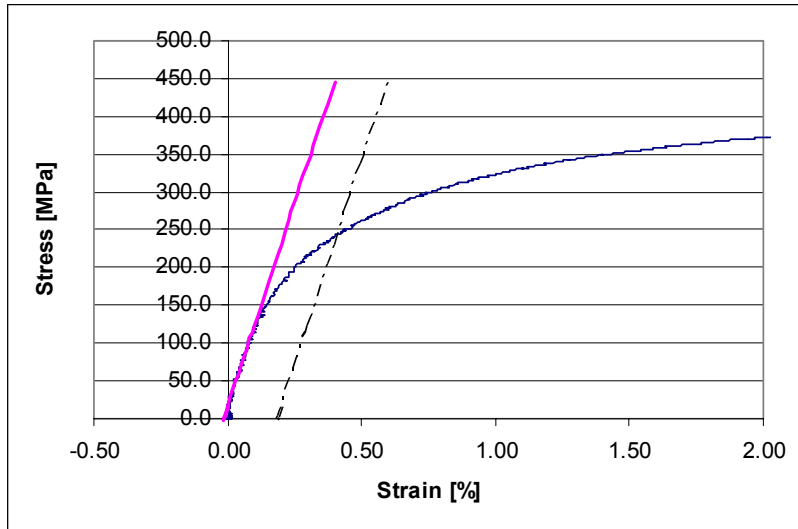
(a)
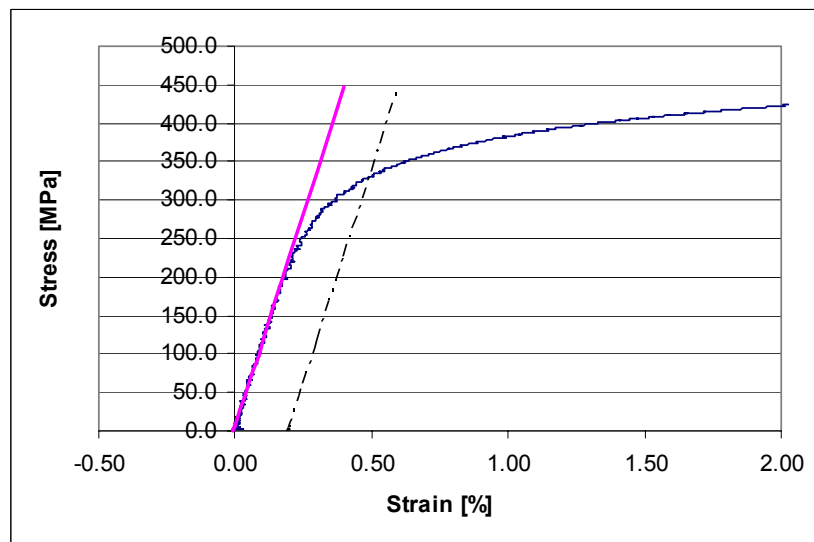
(b)

Figure 3.11: Initial Portion of the Stress-Strain Curves of the Root Region Tests (a) Adjacent to Fracture; (b) At Equivalent Blade Thickness and Location

To assess the amount of work hardening, the curves from these regions were superimposed (see Figure 3.12) and from this method, the estimated plastic strain is about 3%. However, it is also possible that the differences between the curves relate in part to strain hardening and in part to cooling rate and other casting effects – the differing shapes of the post-yield curves and the differing ultimate strengths shown in Table 3.2 provide some evidence for this. This is discussed further in Section 6.
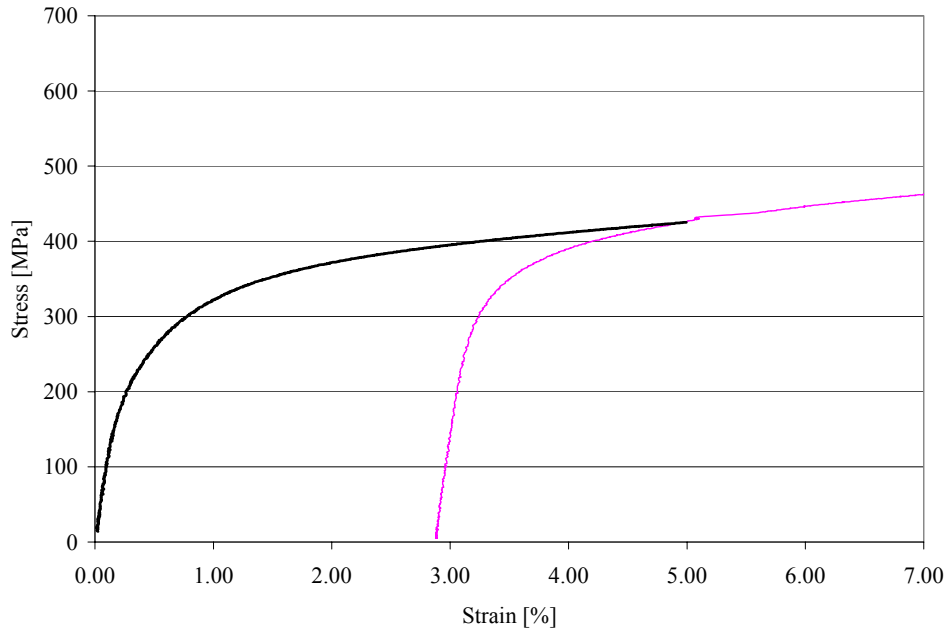
Figure 3.12: Superposition of the Stress-Strain Curves

Other trends from these series of tests are:

- The yield strength of the material at the centre of the blade of the root region is lowest in the mid-thickness region of the largest thickness region. This could be explained by the expected lowest cooling rate in this region.
- The specimens from the mid-thickness and near surface location from the root region of the blade do not have significant differences in the yield strength.

Test Results: Charpy V-notch test results

Impact testing at -10°C was performed in accordance with ASTM E23 1997. The results are reported in Table 3.3.

Table 3.3: Charpy V-Notch Results

Specification or Specimen and Location	Temperature, ($^{\circ}$C)	CVN Absorbed Energies, (J)	Average CVN Absorbed Energy
ABS Type 5 (Superston 70)	-10		≥20 * (Typical ≥30)
Frac (near Surface, adjacent to fracture)	-10	12, 13.5, 12	12.5
SS (near Surface, root region)	-10	12, 13.5, 13.5	13
T/2 (root region)	-10	12, 11.5, 12	12
T/2 (root region, broken line Fig. 9)	-10	11, 11, 12	11

* Based on separately cast bar

The results do not show any significant differences in the toughness of the regions evaluated. The region adjacent to the fracture that is assumed to be plastically deformed does not show any significant loss in toughness. The toughness of the blade is lower than that of specimens machined from separately cast bar, as a result of the significantly faster cooling rate of the latter casting.

4.   TASK 2: FINITE ELEMENT MODELLING

The propeller geometry was determined from Canadian Vickers Drawings MCA-MA-286-130. The propeller sections were only provided for locations up to 0.95R. Therefore, to incorporate the tip of the propeller in the model, the tip shape was estimated by scaling the cross section at 0.95 to 0.99 R to ensure a smooth profile towards the tip. The propeller model was defined semi-parametrically in an ANSYS 7.0 macro. Coordinates extracted from the drawings defining the perimeter of the blade sections were copied into a text file and then incorporated into the macro file.

Construction of the model is depicted in Figure 4.1. First the coordinates were used to generate a series of lines representing the perimeter of the blade sections, in essence creating a skeleton of the blade geometry. Surface areas were created by skinning over the lines and, finally, the blade volume was generated within the surface areas. The model was meshed using 20 noded, SOLID186 brick elements that incorporate quadratic displacement behaviour and are suited to meshing irregular geometries. The elements support plasticity, large deflection, stress stiffening and large strain scenarios.

A multi-linear stress-strain material model was used based on tensile test results from the specimen extracted near the hub region of the broken blade as described in Section 3. The stress-strain behaviour for the model is depicted in Figure 4.2. A value of 0.33 was chosen for Poisson's ratio. As discussed in Section 3, although it is somewhat unclear as to whether this stress-strain curve would have been representative of the properties along the blades prior to deformation, it undoubtedly provides a better basis than the curve near the fracture, which is for a post-yield state.
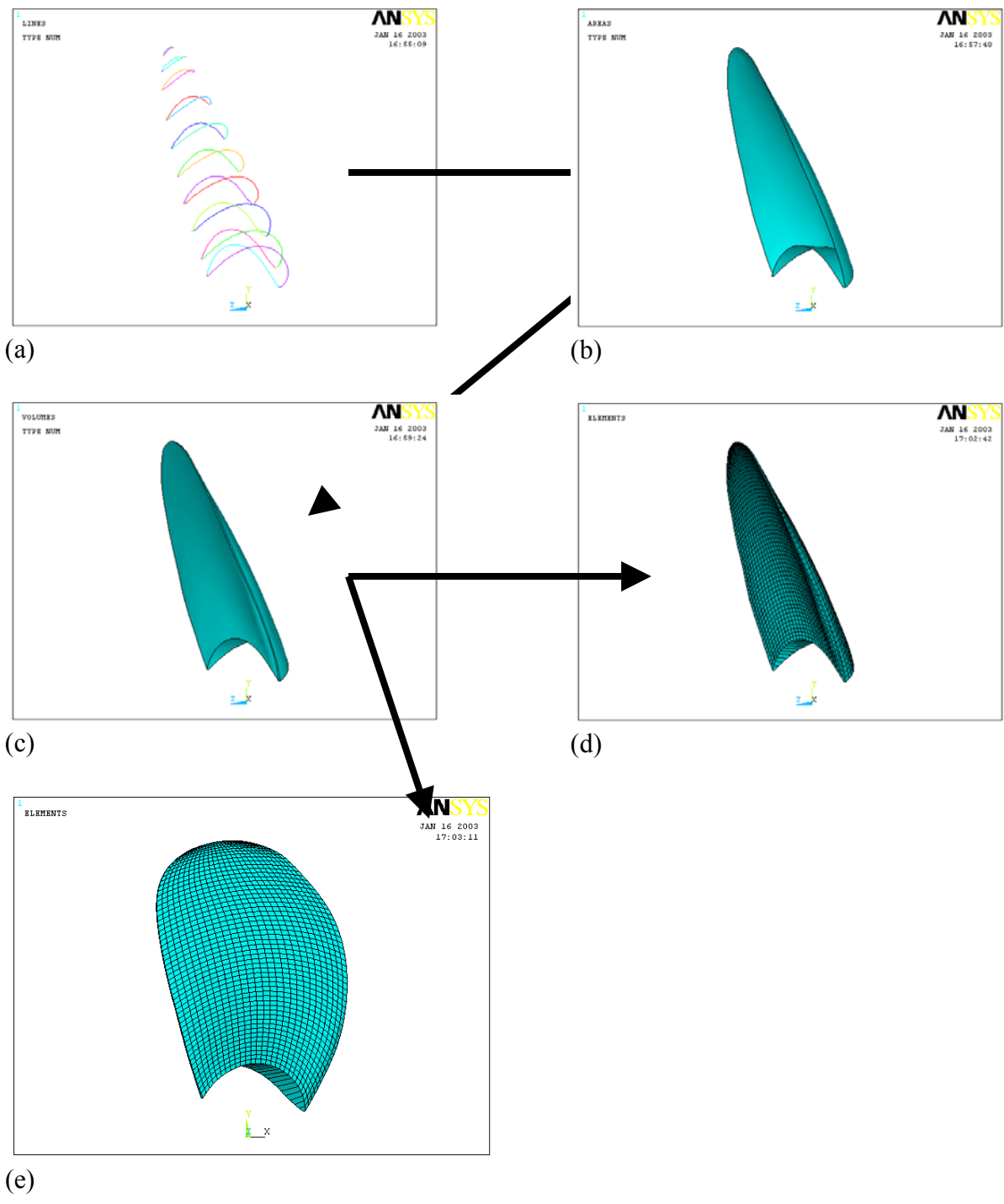
Figure 4.1: FE Model Generation, (a) Lines Defining Section; (b) Areas Generated over Lines, (c) Volume Created from Areas, (d) and (e) Meshed Volumes
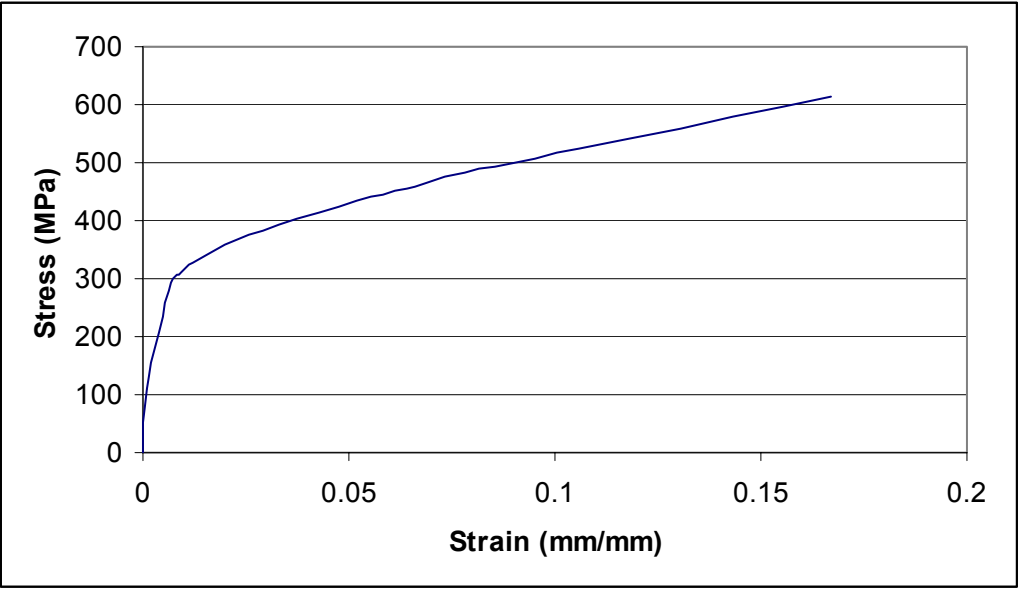
Figure 4.2: Stress-Strain Behaviour of Blade Material Used in FE Models

5.   TASK 5: DAMAGE ANALYSIS AND LOAD DEFINITION

5.1   Damage Characterization

The first step towards damage characterization required measurement of the shape of the blades, as defined by the five moulds described in Section 2. This was done in BMT FTL's Kanata facility, using a multi-axis measuring arm as shown in Figure 5.1.

The Microscribe-3D measuring system has an accuracy listed as 0.38 mm in a 100 point ANSI sphere. It has a 50-in. spherical workspace, and so was moved between measuring locations. To assist with the measurement process, and specifically with maintaining alignment between measurement locations, a grid was established on each blade as shown.

Figure 5.1: Measurement of Blades

The blades were supported at multiple points to minimize any deflections during the measurement process, though the moulds are in any event quite rigid. The Microscribe was connected to a laptop via an RS232 serial interface and data was gathered directly in MS Excel^{TM}. The unit can also export to the Rhinoceros^{TM} software package, which was subsequently used for visualization and fairing, and so the Excel step was not a requirement.

Despite attention to measurement techniques, it was necessary to smooth the data to some extent for all the blades. Figure 5.2 provides an example of the surface created from raw data, indicating some poor data points. The measurement datum plane shows up as an additional horizontal surface.
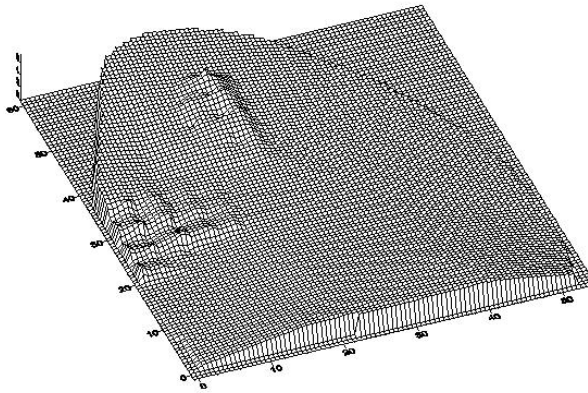
Figure 5.2: Unfaired Mould Model

The most challenging aspect of the damage characterization proved to be the alignment of the mould models with the blade models created for the FEA. In retrospect, several measures should have been taken during the moulding process to mitigate this. At the time, the exercise was conducted in great haste as it was expected that the propellers would shortly be disposed of for scrap.

It had been assumed that the blades did not deform at the connection to the hub, and therefore the moulds could be aligned with the model developed from the drawings at their root. However, the fairing of the blades into the hub is not well defined in the propeller drawings, and could not therefore be included in the FE model. In addition, the moulds themselves are imperfect at their edges, making it very difficult to establish and compare chord lengths or other known dimensions on the original propeller.

A number of mathematical optimization techniques were tried in order to generate an alignment, but in the end the most effective approach proved to be "eyeballing" the matchup using Rhinoceros surface models. Viewed face-on, the mould of the damaged propeller should lie completely (or almost so) behind the undamaged blade, as the stiffness in the chordwise direction is very high. Close to the root of the blade, the original blade and the mould should coincide, or nearly so, and the damaged surface should always be behind the original. At no radius should the mould be longer than the real blade. By respecting these conditions, holding the two surfaces together near the root and rotating, the mould surface could be used to create a reasonable approximation of the true deformed surface. Figure 5.3 provides an example of the final version for one of the propeller blades.
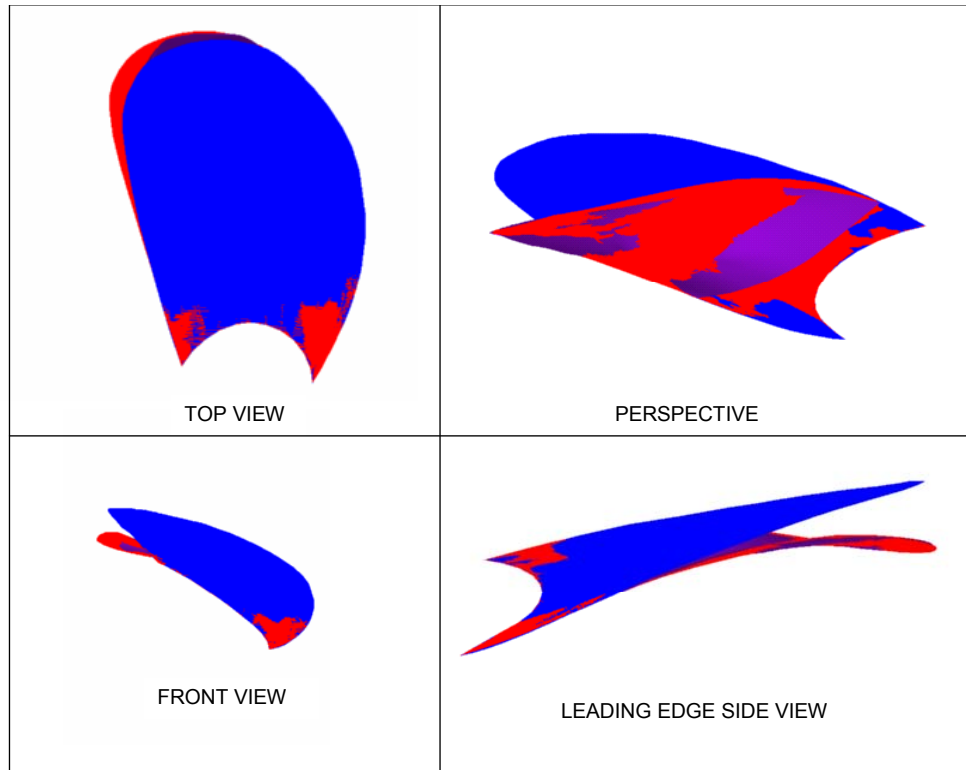
Figure 5.3: Original (Blue) and Deflected Shape (Red) of Blade 1

Some additional checks were also made against the FE models of deformed blades, as certain comparisons could not be physically possible. However, realistically, the total deflections derived in this way could be $\pm$ 10% different from reality.

Table 5.1 summarizes the extent of the blade deformations derived from the moulds. In all cases this was a combination of bending and twisting. The bending essentially defines the progressive and maximum deflection along the axis of maximum thickness, and the twisting the rotation around this axis, though the shapes are somewhat more complex than this. When deriving the loads that caused the deformations, the bending is principally related to magnitude and lengthwise distribution, and the twisting to the chordwise distribution. Figures 5.4 and 5.5 illustrate how the two measurements were derived.

Table 5.1: Summary of Blade Deformations

		Actual from Castings	
Blade		Tip deflection (mm)	Twist at 400 mm from tip (°)
Starboard	1	302.20	5.27
	2	198.14	1.68
	3	193.76	-0.88
Port	4	59.49	-0.92
	5	Broken	Broken
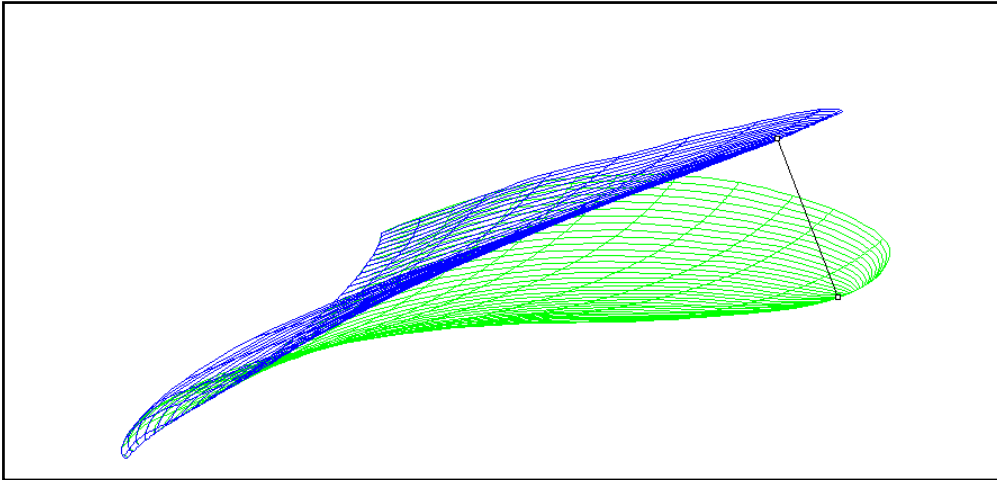
Figure 5.4: Example of Tip Deflection Measurement
Undeflected Blade (Upper Blue); Deflected Blade 1 (Green)

Twist was measured, relative to the undeflected blade, at a location 400 mm towards the hub from each assumed tip. A line was constructed perpendicular to this line and projected to the leading and trailing edges. The relative difference between the original and each deformed blade over the blade width was converted to an angle. Positive twist is defined as greater deflection at the trailing edge than at the leading edge.
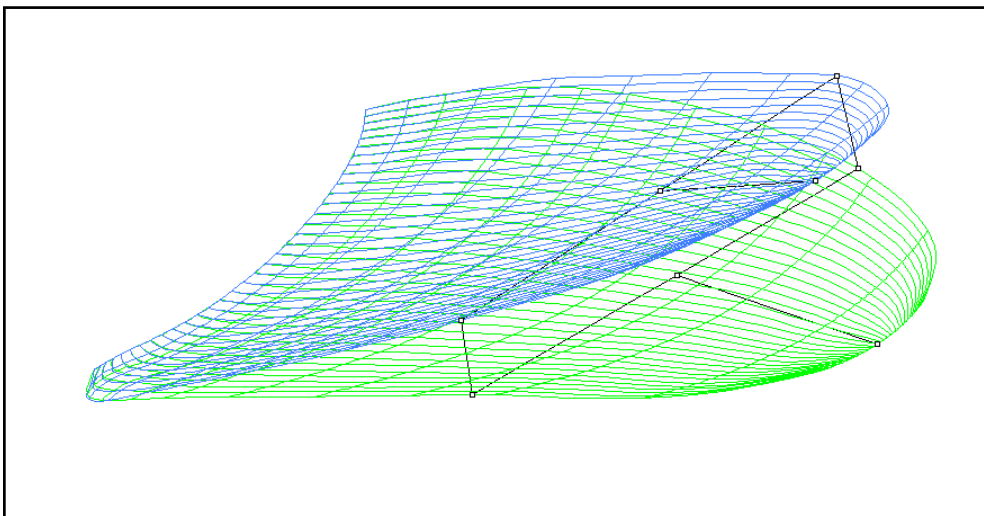

Figure 5.5: Derivation of Twist

5.2　Load Definition

Once a deformed shape had been established with reasonable confidence, FE modelling was used to derive the approximate load and load distribution that might have caused this.

The process used was progressive and iterative. An initial estimate led to a deformed shape that was matched with the deflection and twist of the mould. The load magnitude and distribution were then revised to provide a better match. Once the first blade had been analyzed, the process was easier and faster for each subsequent model.

The bottom of the model was restrained against motion in all directions and pressure loading was applied between various radii (starting at 0.5 R) and the tip of the blade. Two load steps were required. The first load step was used to apply the pressure loading and in the second load step the pressure was reduced to zero to allow for any rebounding due to elastic recovery. The rebound is dependent on the strains due to the loading, due to the shape of the stress/strain curve (Figure 4.2). However, rebounds could be estimated with reasonable accuracy after the first few iterations, which simplified their treatment in subsequent tries.

By observation of the damage, it was expected that the load would need to be applied closer to the trailing edge than to the leading edge of each blade. Initially the blades were loaded over 50% of the chord forward from the trailing edge, and this extent was subsequently modified to improve the fit.

Initially, the load was modelled as a constant pressure over the entire loaded area. Once a reasonable match was found, this was modified to include pressure gradients at each edge of the patch, to provide a slightly better representation of ice-crushing physics. The location and size of the region of the peak pressure were selected using several iterations. After each model was solved, the predicted rebounded blade deformation was compared to the mould measurements. Depending on how well the two data sets compared, modifications were made to the loading until an acceptable match was achieved. Figure 5.6 shows the match achieved for Blade 1.

The number of load iterations required for the first blade modelled was around 30, although this included tests with a number of mould/blade alignments in addition to mould/model matching. For the other blades 5 to 10 iterations were required to achieve good matches.
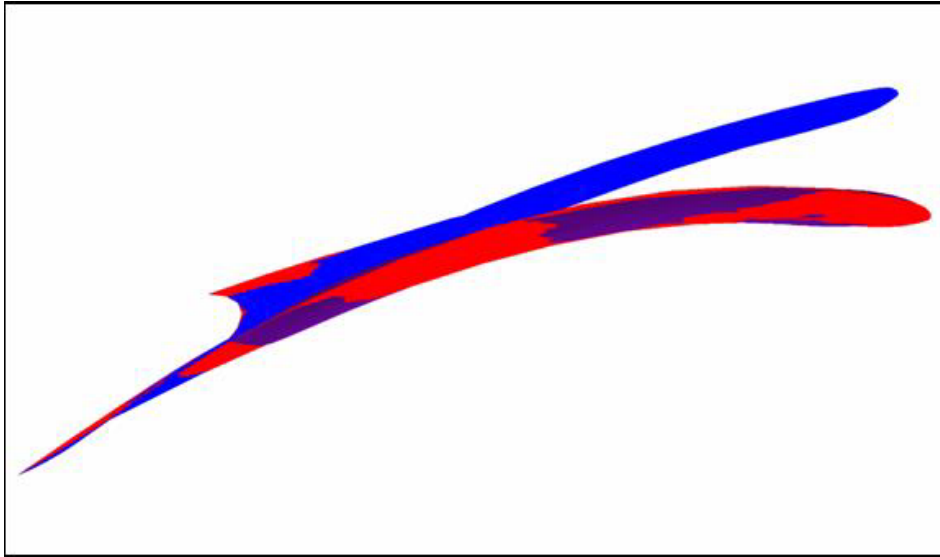
Figure 5.6: Original Starboard Blade + Blade 1 Casting + FEA Rebounded Model

For all of the blades, the best match of analytical results to the moulded shapes was found with pressure patches over part of the chord from the trailing edge to the centre of the propeller and extended from 0.75 R out towards the tip. The peak pressure in all cases was selected as 13 MPa, over areas that varied between 0.295 m and 0.46 m. The total applied force thus varied from 2.23 MN to 3.69 MN as shown in Table 5.2.

Table 5.2: Summary of Applied Loads

Blade		Loaded Area (m^2)	Average Pressure (MPa)	Total Load (MN)
Starboard	1	0.460	8.04	3.68
	2	0.295	9.22	2.92
	3	0.356	9.22	3.28
Port	4	0.432	5.16	2.23

Comparing Tables 5.1 and 5.2, it can be seen that Starboard Blade 1 has the greatest deflections and the highest loads. However, the second highest total load is on Starboard Blade 3, which had a smaller deflection than Starboard Blade 2 and less (and opposite) twist. This is a consequence of the thicker sections towards the leading edge, which apply more resistance to the applied loading.

FE model solutions were generated for three deformed starboard blades (Starboard Blades 1, 2 and 3) and one port blade (Port Blade 1). The pressure loading and residual strains are given for each blade in Figures 5.7 to 5.10. The strain component presented is the Y-direction strain (radially outward) along the blade, or in essence the bending strain component. This component of strain identifies regions of tensile and compressive plastic deformation.

It can be seen that in all cases the plastic deformation (strains) extend over much of the propeller, from root to tip. Thus, the total deflection listed in Table 5.1 is the result of accumulation of deflection along the length of the blade rather than damage concentrated at the tip – this can also be seen in the comparisons of original and deflected shapes. There is a tendency for the leading and trailing edges to show higher residual strains than the centre of the blade.

(a)

(b)

(c)

Figure 5.7: (a) and (b) Residual Strains Resulting from (c) Applied Pressure Loading (MPa) for Starboard Blade 1

(a)

(b)

(c)

Figure 5.8: (a) and (b) Residual Strains Resulting from (c) Applied Pressure Loading (MPa) for Starboard Blade 2
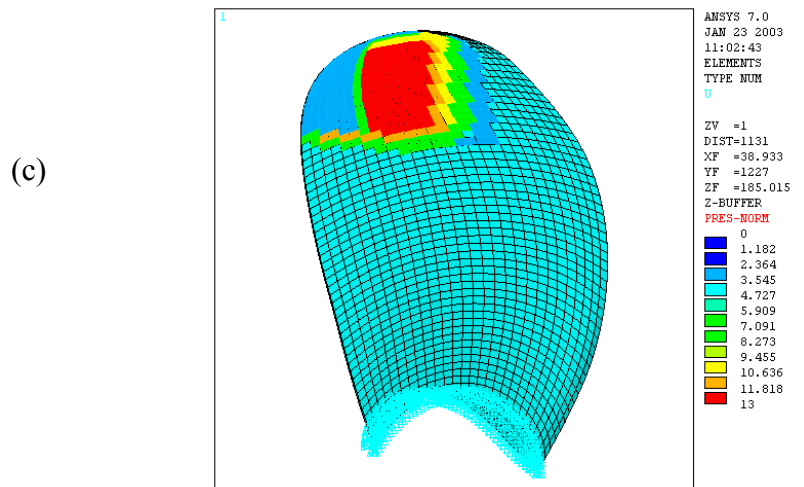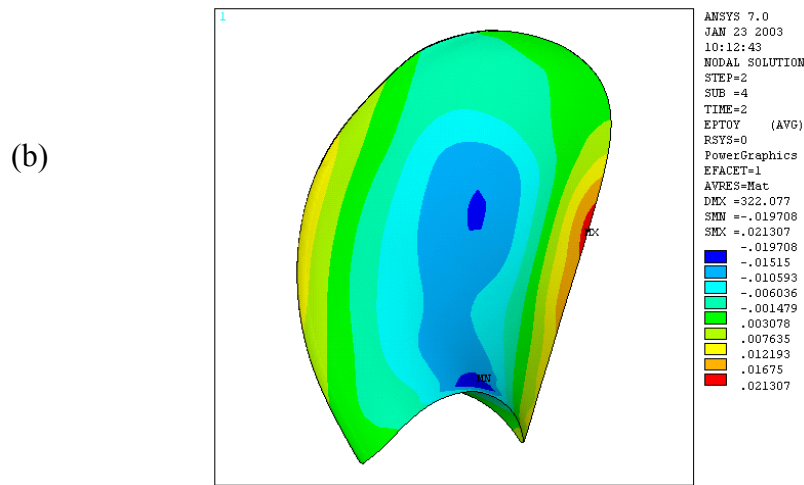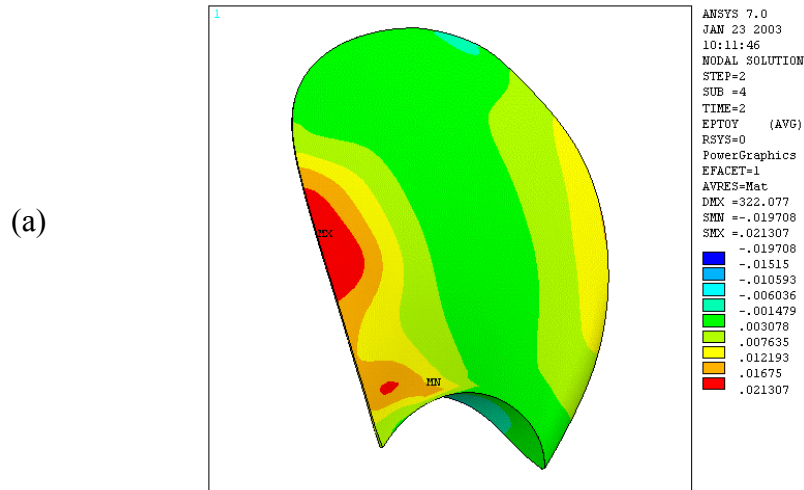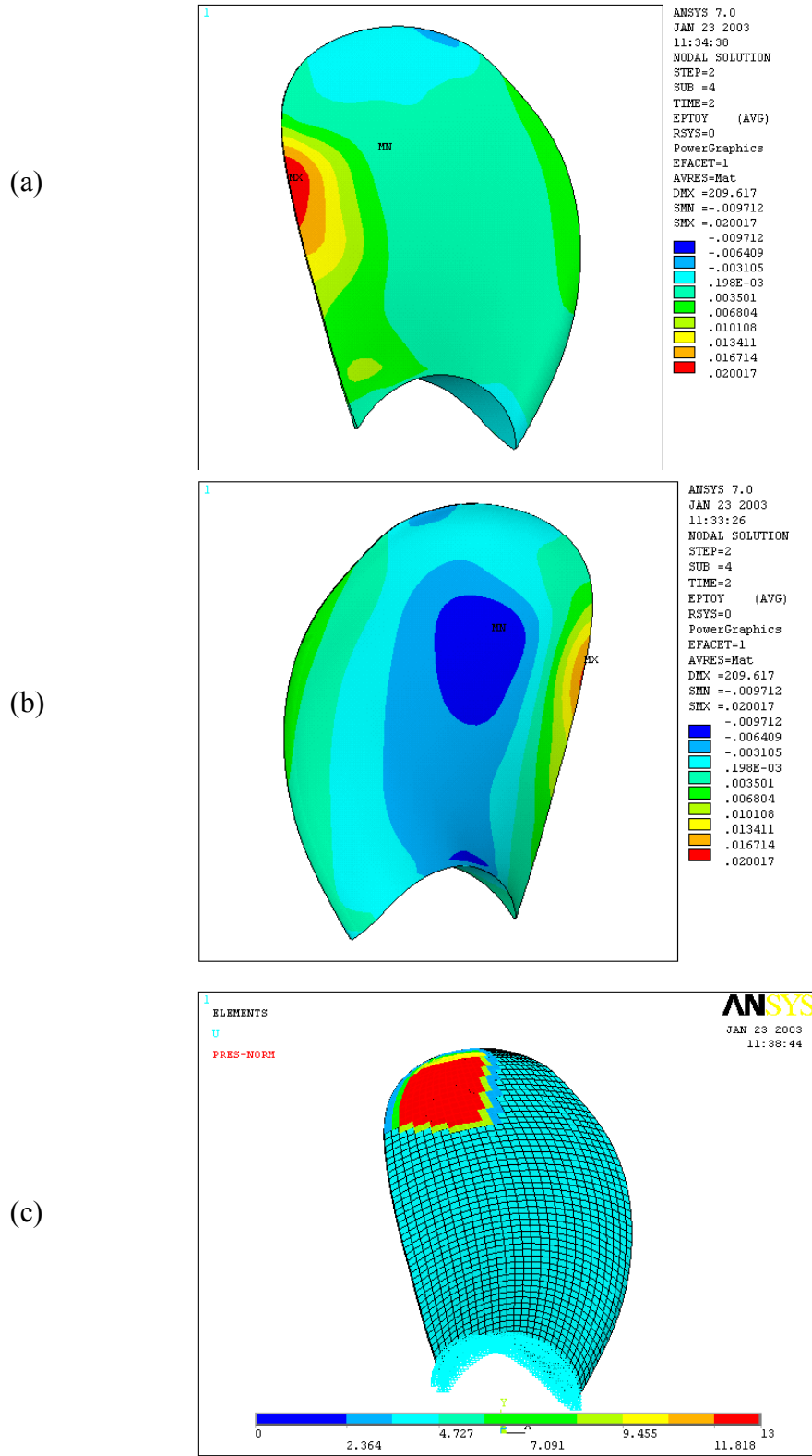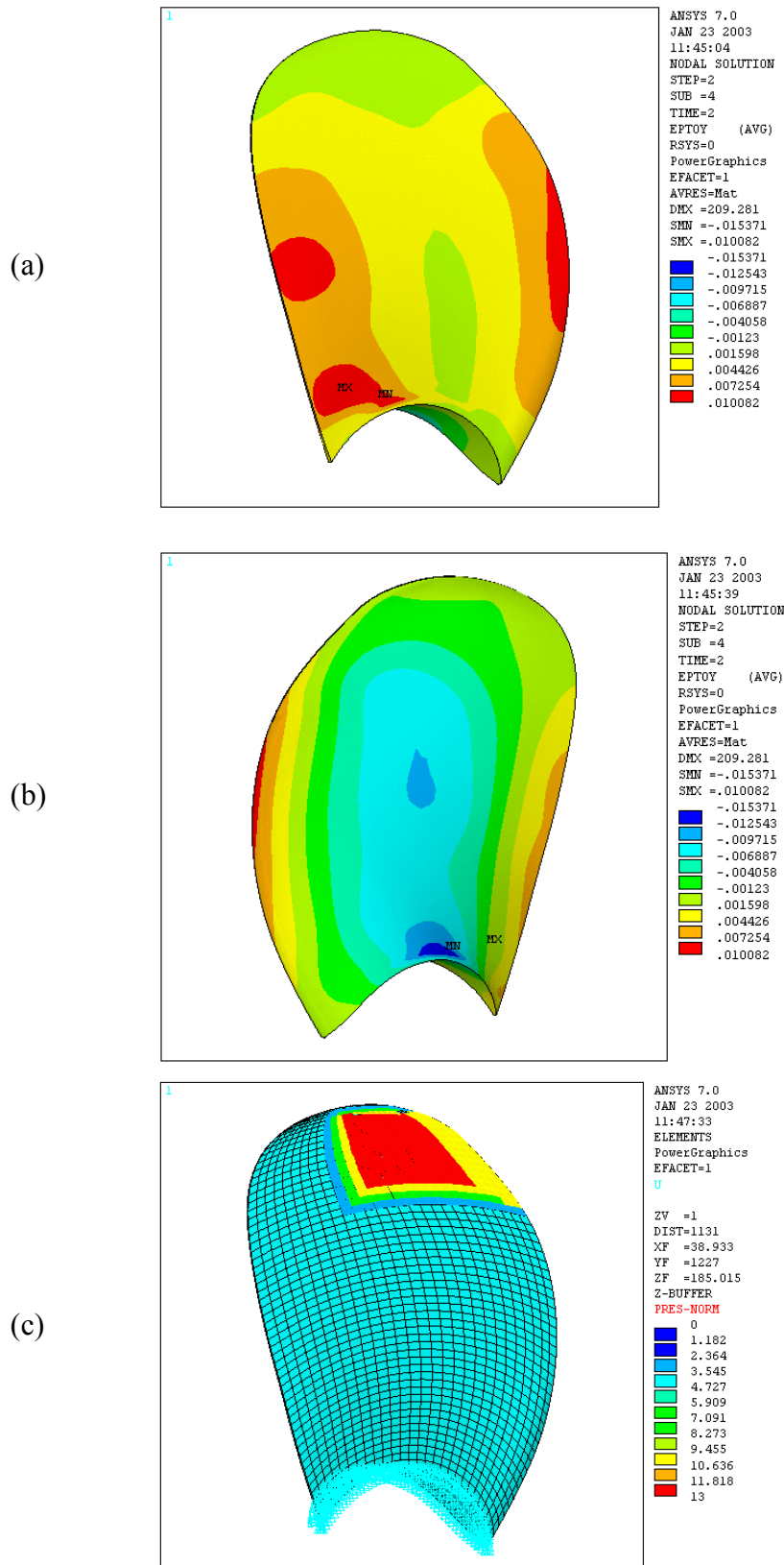
Figure 5.9: (a) and (b) Residual Strains Resulting from (c) Applied Pressure Loading (MPa) for Starboard Blade 3

(a)

(b)

(c)
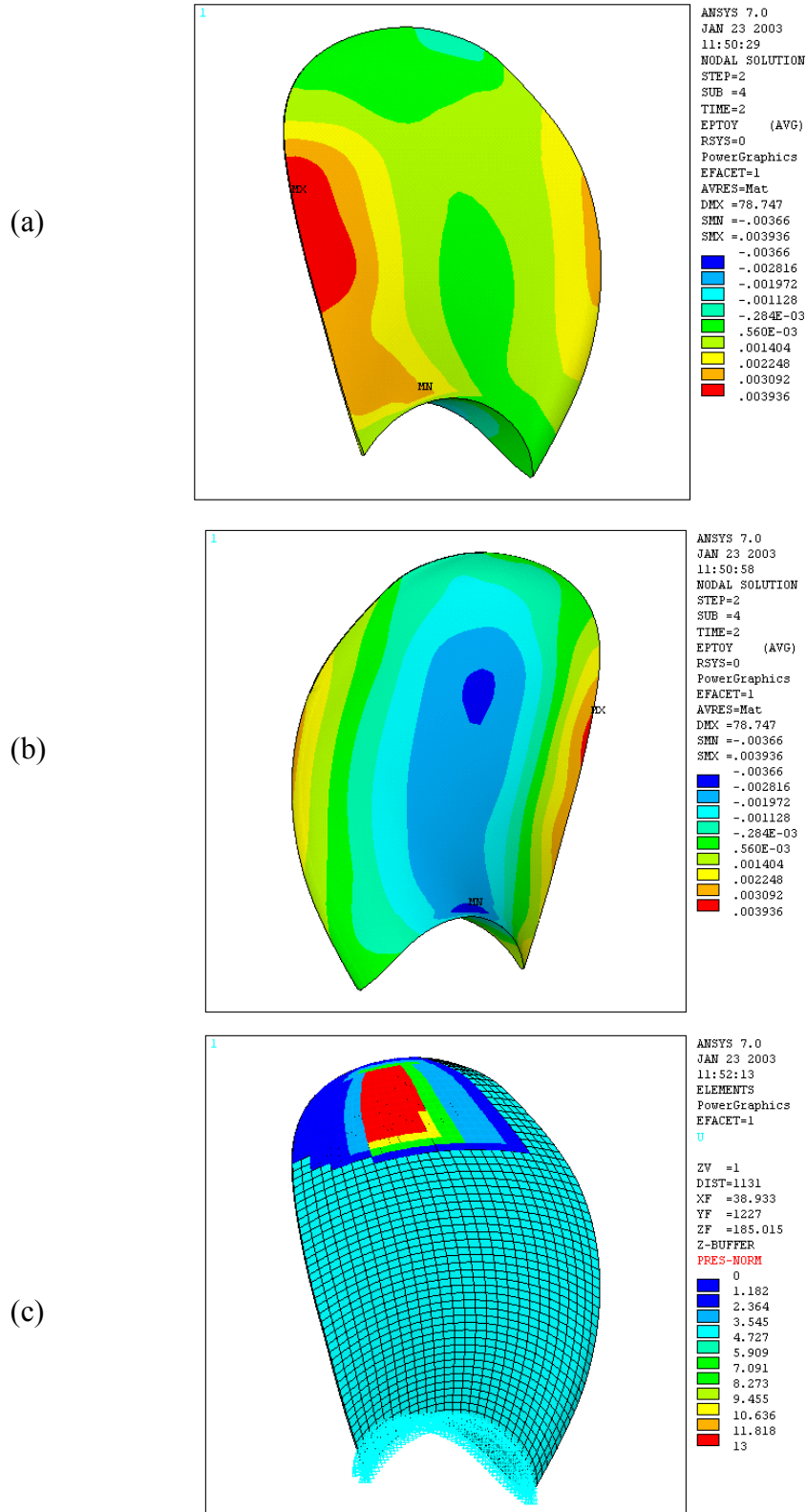
Figure 5.10: (a) and (b) Residual Strains Resulting from (c) Applied Pressure Loading (MPa) for Port Blade 1

32

Residual strain is important to the continued serviceability of the propellers, but the stresses of most importance to failing the blades are those at the time of application of the load. Two sets of stress distributions for Starboard 1 and 3 are shown in Figures 5.11 and 5.12. The blades are essentially cantilevers, and therefore the face is put into tension and the back into compression by the load patterns deduced from the models. Table 5.3 shows the peak tensile and compressive stresses (von Mises stresses) for each blade.

Figure 5.11: Blade 1 Stress Contours

```
1                                          ANSYS 7.0
                                           FEB  6 2003
                                           11:12:48
                                           NODAL SOLUTION
                                           STEP=1
                                           SUB =7
                                           TIME=1
                                           SEQV    (AVG)
                                           PowerGraphics
                                           EFACET=1
                                           AVRES=Mat
                                           DMX =286.111
                                           SMN =29.469
                                           SMX =382.485
                                              29.469
                                              68.693
                                              107.917
                                              147.141
                                              186.365
                                              225.589
                                              264.813
                                              304.037
                                              343.261
                                              382.485
```
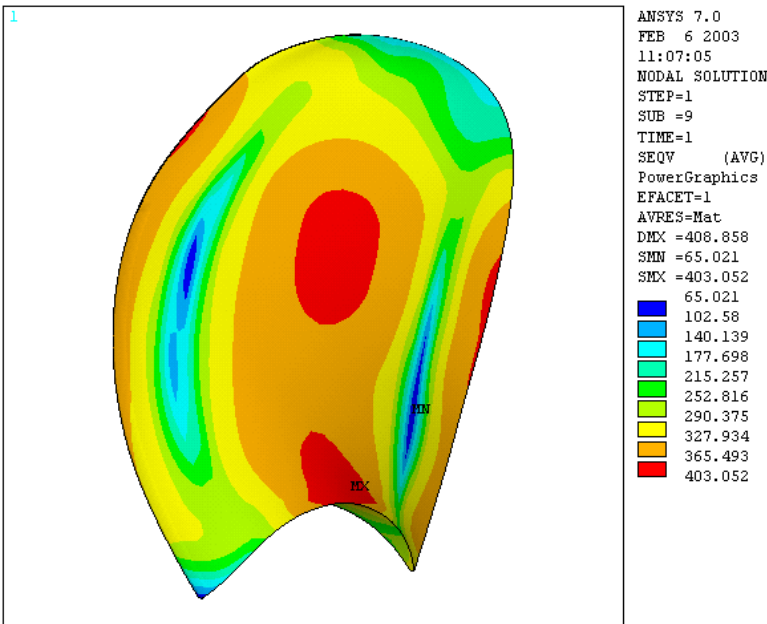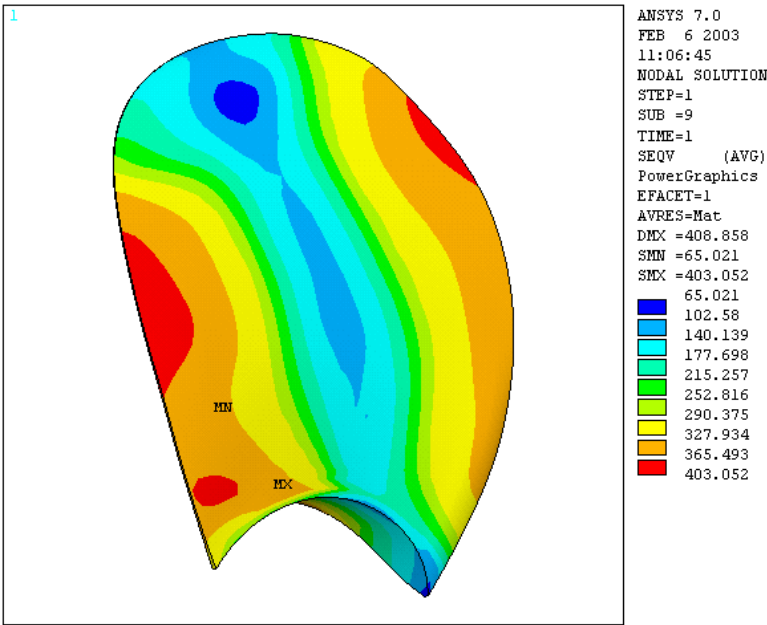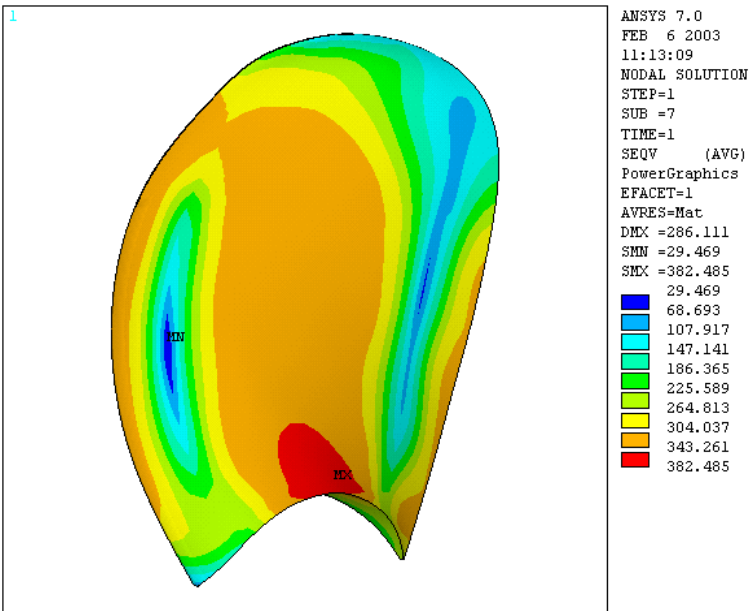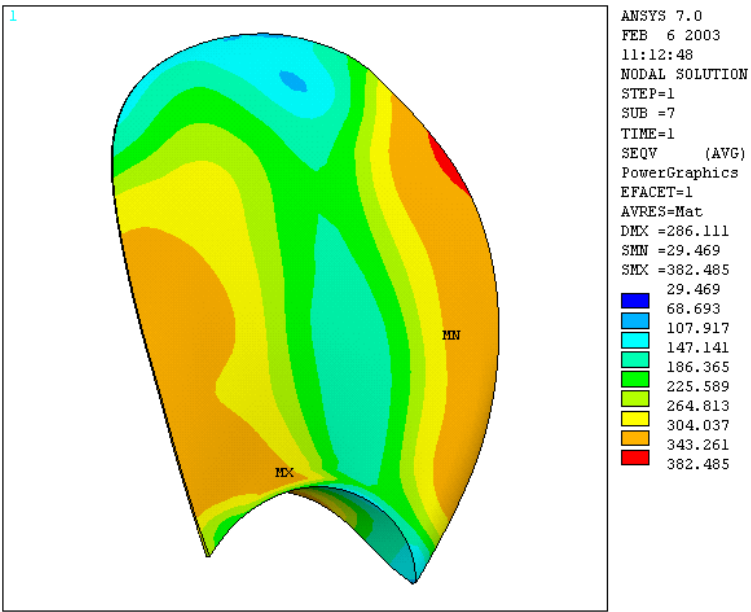
```
1                                          ANSYS 7.0
                                           FEB  6 2003
                                           11:13:09
                                           NODAL SOLUTION
                                           STEP=1
                                           SUB =7
                                           TIME=1
                                           SEQV    (AVG)
                                           PowerGraphics
                                           EFACET=1
                                           AVRES=Mat
                                           DMX =286.111
                                           SMN =29.469
                                           SMX =382.485
                                              29.469
                                              68.693
                                              107.917
                                              147.141
                                              186.365
                                              225.589
                                              264.813
                                              304.037
                                              343.261
                                              382.485
```

Figure 5.12: Blade 3 Stress Contours

Table 5.3: Peak Stresses

Blade		von Mises Stress (MPa)
Starboard	1	403
	2	378
	3	382
Port	4	312

Other implications of the results are discussed at Section 6.

6. DISCUSSION OF RESULTS

6.1 Loading

Figure 6.1 illustrates one of the loadings assumed in the IACS Unified Requirements for Polar Ships [3]. In both cases, these loads are to be applied to the back of the blade. Both design loads relate to contact while the ship is moving forward.

Figure 6.1(a). Contact area on the blade for leading edge loading.	*Figure 6.1(b). Contact area on the blade for tip loading.*
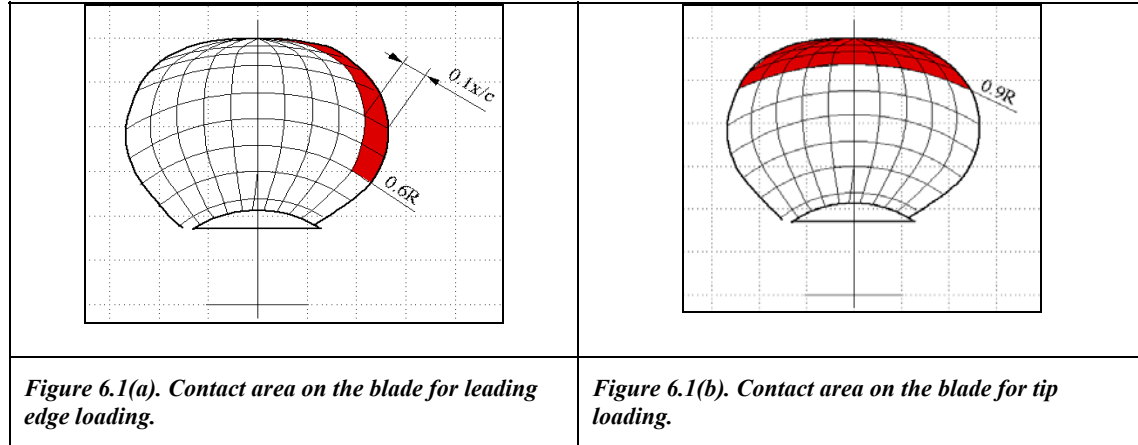
Figure 6.1: IACS Load Model for Back Loads

Figure 6.2 illustrates the IACS model for face loads. This is again related to an assumed loading mechanism due to milling while moving forward.
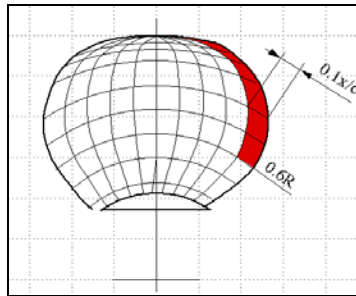
Figure 6.2. Contact area on the blade for leading edge loading.

Figure 6.2: IACS Load Model for Face Loads

The magnitudes of the IACS loads are derived by a set of formulae that relate load to the ship's polar ice class, propeller dimensions, and rotational speed, as shown below for the back loading case in Figure 6.1(a):

when $D < D_{limit,}$

$$F_b = -33.4 S_{ice} [nD]^{0.7} \left[\frac{EAR}{Z} \right]^{0.3} [D]^2 \text{ kN} \tag{6.1}$$

36

when $D \geq D_{limit}$,   (also applies when D=D limit)

$$F_b = -29.2 S_{ice} [nD]^{0.7} \left[\frac{EAR}{Z} \right]^{0.3} (H_{iclass})^{1.4} D \quad kN \tag{6.2}$$

where $D_{limit} = 0.873 *(H_{iclass})^{1.4}$
$S_{ice} = 1.2$ MPa (polar class 3 ship)
$H_{iclass} = 3$ m (polar class 3 ship)
n = rotational speed (per second)
D = propeller diameter
EAR = expanded area ratio
Z = number of blades

For the *Louis*, the force derived from this is approximately 2105 kN.

For forward bending (Figure 6.2) the relevant formula is:

$$F_f = 628 \frac{1}{\left(1 - \dfrac{d}{D}\right)} H_{icllass} \left[\frac{EAR}{Z} \right] D \quad kN \tag{6.3}$$

This gives a total force of 2060 kN.

Under any force and loading, the calculated blade stresses should not exceed:

$$\frac{\sigma_{ref}}{\sigma_{calc}} \geq 1.3 \tag{6.4}$$

σ_{ref} is reference stress, defined as:

$\sigma_{ref} = 0.7 \cdot \sigma_u$ or
$\sigma_{ref} = 0.6 \cdot \sigma_{0.2} + 0.4 \cdot \sigma_u$ whichever is lesser.

The nominal values for $\sigma_{0.2}$ and σ_u, taken from Table 3.2 are 310 MPa and 690 MPa, respectively, giving σ_{ref} as 462 MPa. Thus a design value of σ_{calc} should be in the order of 355 MPa. However, if the actual values for $\sigma_{0.2}$ and σ_u, as used in the FE model are used (245 MPa and approximately 500 MPa, respectively), σ_{calc} should be 267 MPa.

Figures 6.3 to 6.5 show the von Mises stress contours resulting from the three load cases. There are some difficulties in applying the UR load model due to the step changes from 0 to maximum pressure, and these result in some local stress concentrations, particularly for the leading edge applications. When these are discounted, the most severe loading case is found to be the tip load (Figure 6.3(b)), with peak stresses of approximately 345 MPa. This value lies between the nominal and actual design values derived above, indicating that the propeller design would have been evaluated as marginally adequate for a PC 3 ship, if the nominal material properties were assumed, and quite inadequate if actual properties were used.
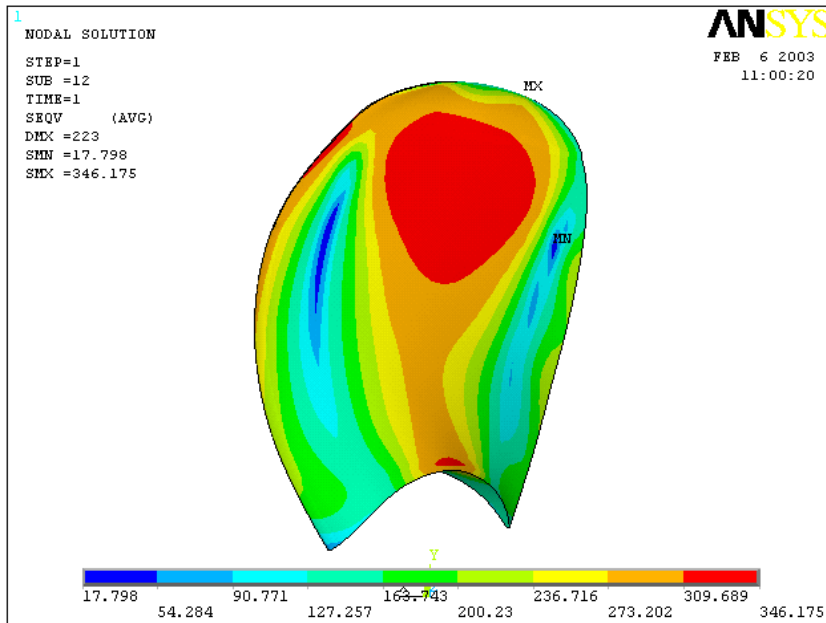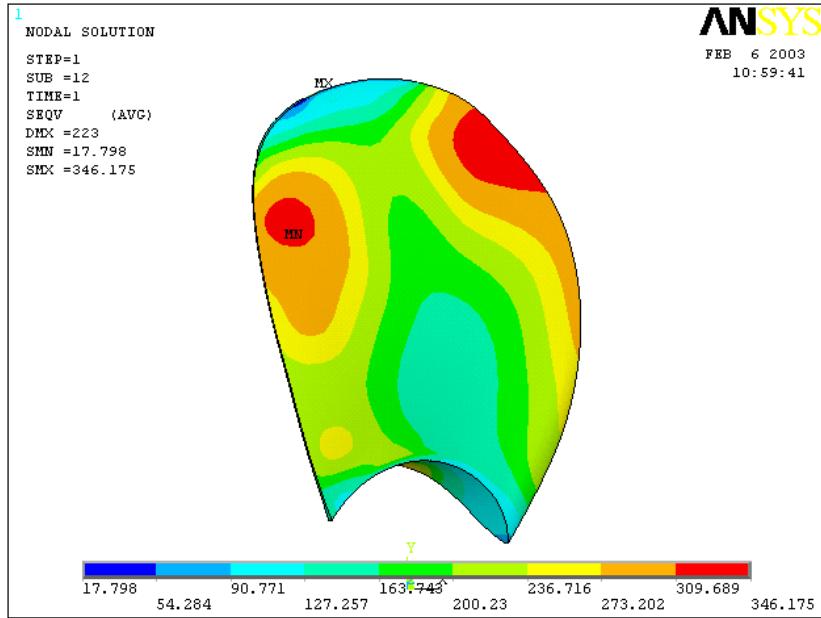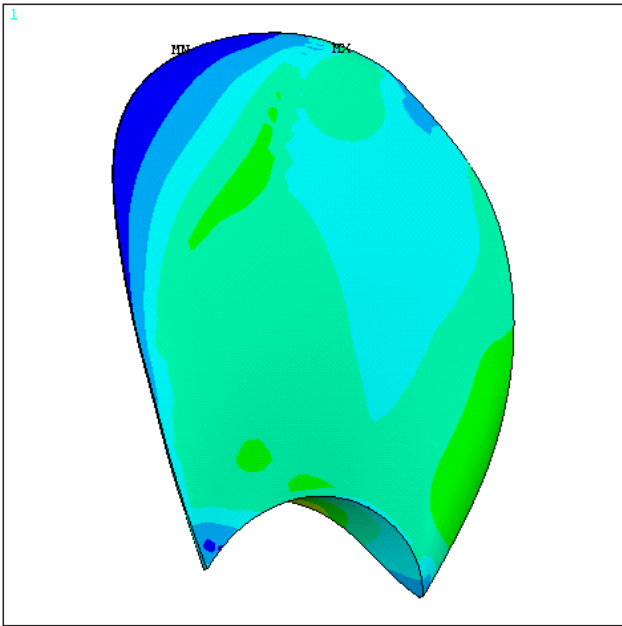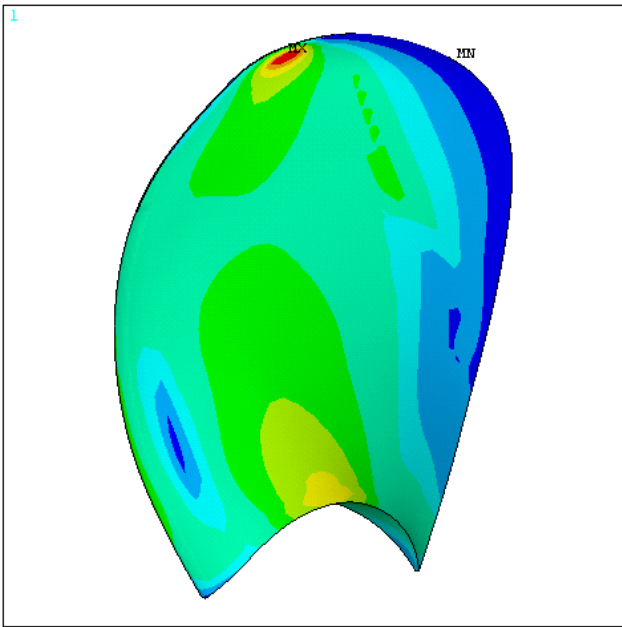
Figure 6.3: UR Load Applied to Tip of Suction Side

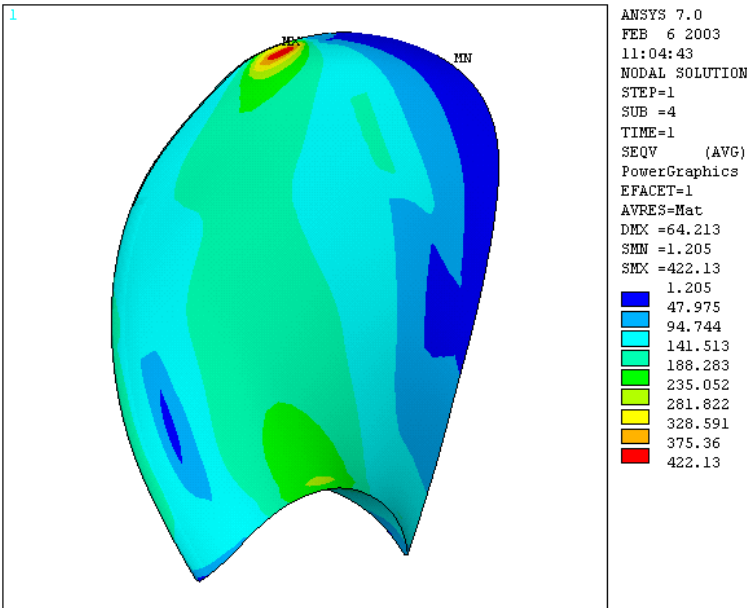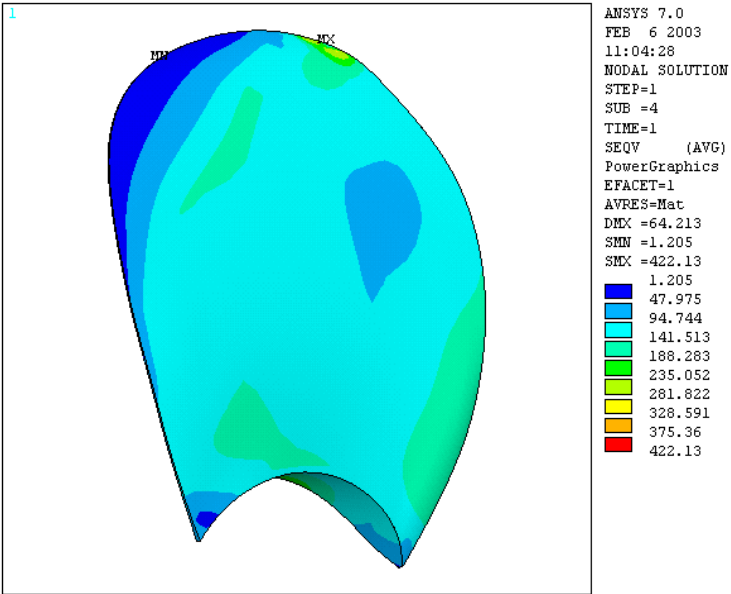**Figure 6.4: UR Load Applied to Leading Edge of Suction Side**

Figure 6.5: UR Load Applied to Leading Edge of Pressure Side

Comparing these load models with the damage loads derived in Section 5, it can be seen that the *Louis* propellers were damaged by a wholly different mechanism. In all cases, the load is applied towards the trailing edge of the blades rather than at the leading edge, and is more distributed than the IACS load model. Load is very definitely applied to the face (pressure side) rather than to the back (suction side) of the propeller.

The location and distribution of the actual loads indicates that the *Louis* encountered the ice while moving astern, and with the propellers either stopped or rotating slowly in the astern direction. The ship may have encountered a large multi-year floe, which would have damaged a rotating propeller sequentially, or a consolidated ridge extending to the full draft of the ship, which would have damaged all blades simultaneously. It is not possible to be more definitive about the loading scenario without additional information, which the results of the video studies may eventually provide. However, it is considered probable that all damage came from a single event, as the effects of the damage on ship performance would have been noticeable.

The loaded areas and peak pressures derived from the FE models (Table 5.2) are of scientific interest, as few (if any) comparable measurements have ever been obtained. Figure 6.6 presents a compendium of ice loading data for ships and offshore platforms, presented in the form of pressure versus area plots. The *Louis* data has been added to the plot and it can be seen that the data falls in what might be considered to be an "expected" range of values for impact loads with strong, thick ice. This is an interesting result with implications for both propeller design and appendage design.
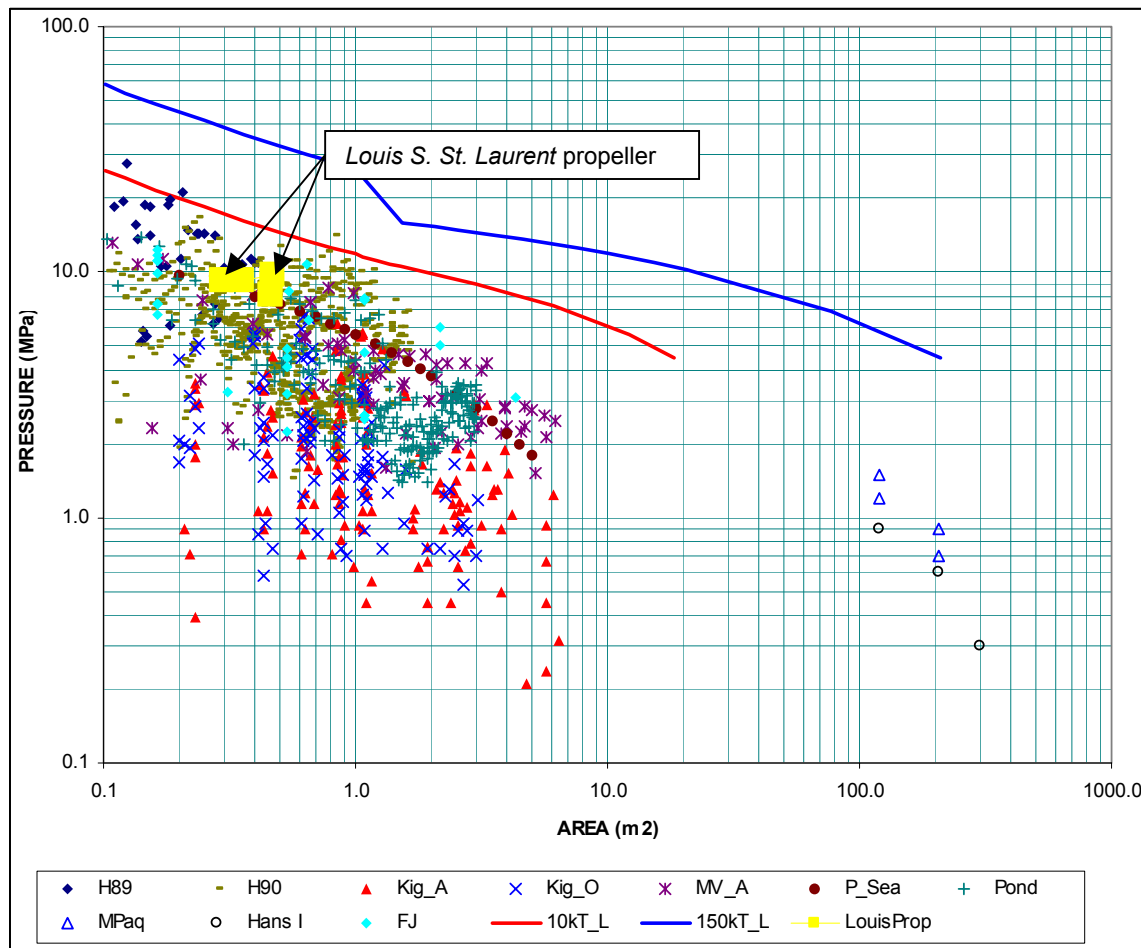

Figure 6.6: Comparison of *Louis S. St. Laurent* and Other Load Data

6.2   Failure Mechanisms

The blade fracture reported in Section 3 could not be tied into a good estimate of failure load due to the difficulty of matching a partial blade mould to the original propeller geometry. It is therefore somewhat unclear whether this blade broke due principally to the casting imperfection found by the investigation or due to seeing a very high overall load.

As noted above, all the blades for which loadings could be derived saw stresses considerably in excess of yield and much of the way towards ultimate for the propeller material. A comparison can be made of where the failure initiated with the locus of maximum stress on Blade 1, the most deformed of the unbroken blades, as shown in Figure 6.7.
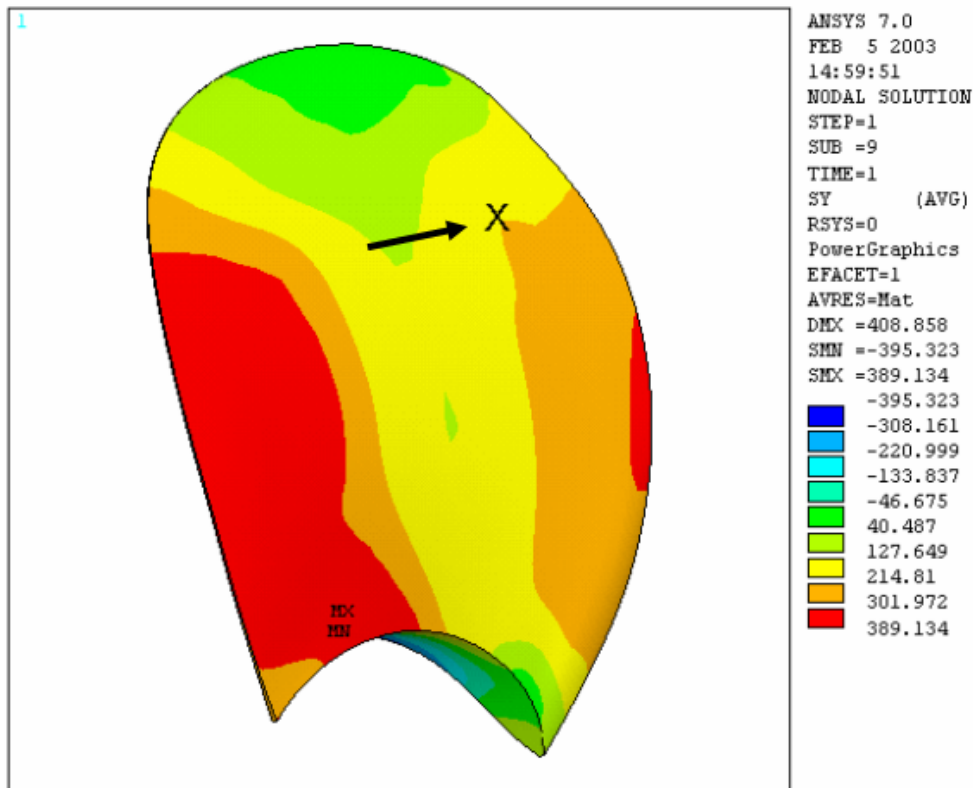

Figure 6.7: Approximate Location of Initial Fracture and Stress Distribution from Blade 1

This suggests that the fracture initiation point was not far from being the most highly stressed point on the blade. Therefore, local stress concentrations around the inclusion may have led to fracture initiation, but the blade was already significantly overloaded and had presumably deflected to an extent that would have required its replacement regardless of whether the final fracture damage had occurred.

The deflected shapes of the other blades are reasonably consistent, and all point towards an ice crushing load applied as the ship backed into a massive feature. The load was sufficient to bring most of the blade (in the worst cases) well into the plastic range, with the result that significant residual deformations were generated. These included both deflections and rotations of the blades sufficient to require propeller replacement even when blades remained unbroken.

6.3   Forensic Analysis Methodology

The set of techniques used in this project have demonstrated their potential to provide insights into propeller loading and response. New technologies, such as laser scanning may, in the future, offer more accurate means of measuring shape than the moulding technique used in this project. However, in the short term, the moulds provide a relatively simple and reasonably accurate means of deriving post-yield geometry. Any future projects should, however, devote more attention to selecting datum points on the hub and at the blade roots to facilitate the matching of the moulds to the propeller model.

The absolute accuracy of the loads derived from this methodology is limited by a number of factors, the most important of which are:

- Shape measurement accuracy;
- Blade modelling accuracy;
- Material property estimation.

The mould measurements are probably good to within $\pm$10% for the blades as a whole, although some areas at the tip and leading and trailing edges are likely to be worse than this due to a fall-off in rigidity of the moulds at their edges, and to loss of shape definition right at the edges of the moulds. The 10% value is more representative of the resulting accuracy in load estimation.

The blade models assume rigid connections at the propeller hub. This is somewhat conservative, as the yield patterns derived for the blades suggest that there may have been some rotation. The overall influence on load and response is still likely to be relatively small.

The accuracy of the stress-strain curve used in the model is more questionable. As noted in Section 3, a straightforward comparison of the root and tip (fracture surface) curves indicated that the latter might have seen a 3% strain (Figure 3.12). The FE models, however, show residual strains considerably less than this for even the most deformed blade. This discrepancy suggests that the blade yield strength did vary significantly along the length of the blade, and that the estimates of loads may therefore be non-conservative. A single "worst case" comparison for Blade 1, using the stress-strain curve of Figure 3.11(b) gives a total load of approximately 4.6 MN, or 125% of the lower bound estimate. Peak stresses generated by this load are also roughly 125% of those presented in Section 5. However, these are not realistic comparisons, as the stress-strain curve at the hub is known to be closer to that of Figure 3.11(a), and there is undoubtedly some degree of strain hardening built into Figure 3.11(b) due to the failure mechanism.

It can also be noted that there was some degree of strain at almost all propeller radii, as shown in Figures 5.7 to 5.10. Therefore, even the material properties from Figure 3.11(a) may not represent the initial elastic behaviour of the material exactly. However, by taking samples close to the neutral axis of the blade, the degree of strain and strain hardening present is reduced.

Unfortunately, there is no simple way of establishing the "true" distribution of material properties within the propeller, and thus increase confidence in the damage load estimates. Additional material samples could be taken from one of the damaged blades, and an iterative approach could be used to derive the as-built properties. The stress-strain curves of the samples would be corrected using strain estimates derived from the deflected shapes. The overall model would then be re-run, using varying material properties, and strain would be re-estimated. Further corrections to the curves and load model would be made as necessary. The main cost associated with this approach would be in obtaining the additional material samples, due to the size of the propeller.

It should be noted that this material property issue is equally or more important to any analyses of elastic behaviour, as planned in the video/laser monitoring project noted earlier. Again, comparison of the stress-strain curves of Figure 3.11 shows that the same stress could be associated with a doubling of elastic strain, and an even greater variability in deflection, depending on which curve is more representative of the overall propeller properties.

One additional factor should be considered, and that is the possibility that the propellers had previously suffered damage during other overload events. In this case, the load pattern and intensity required to generate the final deflected shape might have been significantly different. We have no means of assessing the likelihood of this, other than the fact that there appears to have been no perception aboard the ship that any such damage had been incurred. The video system data records may be very valuable in confirming propeller condition, as a datum distance was (presumably) established prior to the trials.

7.   SUMMARY AND CONCLUSIONS

The port and starboard propellers from the *Louis S. St. Laurent* were modelled in their intact and damaged conditions, using materials properties taken from actual blade samples, intact shape from the propeller drawings, and damaged shape from a set of rigid moulds taken from the blades.

Loads required to cause the damage were derived using non-linear finite element analysis. The loads were reasonably consistent with each other, and appeared realistic when compared with other ice load data. They were somewhat higher than, and very differently distributed from those assumed in the JRPA 6 program and in the new design rules derived from this. The loads appear to have resulted from backing into heavy ice with propellers turning slowly. This is not a design condition in the Rules, but has long been recognized to be a dangerous scenario. Training and guidance for operators should emphasize the risks of astern operation.

One blade fractured under the load, with the fracture initiating at a casting defect in a highly stressed area of the blade. There was no evidence that fatigue contributed to the failure. It is probable that the local stresses at fracture exceeded the design values established by the IACS Unified Requirements.

Work on the project has shown again that the bronze material used in these and many other icebreaker propellers is highly variable in its properties, and in general is weaker than its nominal specifications. This has implications both for design and for analysis of performance. It is crucial that design calculations incorporate realistic values for material properties.

The forensic analysis toolset used in the project was shown to be capable of deriving a good understanding of damage mechanisms and reasonably confident estimates of damage loads for bending damage. In the future, if other propellers are damaged by ice milling or other "design-type" scenarios, the toolset would be able to test the loading assumptions in design rules more directly.

REFERENCES

[1]   Timco, G.W., and Morin, I. Canadian Ice Regime Database, NRC Report HYD-TR-024, 1997.

[2]   Finnish Maritime Administration Regulations on the Structural Design and Engine Output Required of Ships for Navigation in Ice, "Finnish Swedish Ice Class Rules" Chapter 6, Helsinki, September 2002.

[3]   International Association of Classification Societies Draft Unified Requirements for Polar Ship Machinery, London, July 2000.

[4]   Jones, S.J., et al., Propeller-Ice Interaction, SNAME Transactions Vol. 105, pp 399-425, 1997.

[5]   Investigation on the damaged propeller on the CCGS Louis S. St. Laurent, BMT FTL Report 4409C-5, March 1996.